

A Robust Numerical Method for Generalized Coulomb and Self-Polarization Potentials of Dielectric Spheroids

Changfeng Xue¹ and Shaozhong Deng^{2,*}

¹ Department of Fundamental Sciences, Yancheng Institute of Technology, Yancheng, Jiangsu 224003, China.

² Department of Mathematics and Statistics, University of North Carolina at Charlotte, Charlotte, NC 28223-0001, USA.

Received 4 October 2009; Accepted (in revised version) 30 November 2009

Available online 12 March 2010

Abstract. By utilizing a novel quasi-harmonic three-layer dielectric model for the interface between a dielectric spheroid and the surrounding dissimilar dielectric medium, a robust numerical method for calculating the generalized Coulomb and self-polarization potentials of the dielectric spheroid is presented in this paper. The proposed numerical method can not only overcome the inherent mathematical divergence in the self-polarization energy which arises for the simplest step-like model of the dielectric interface, but also completely eliminate the potential numerical divergence which may occur in other treatments. Numerical experiments have demonstrated the convergence of the proposed numerical method as the number of the steps used to discretize the translation layer in a general three-layer dielectric model goes to infinity.

PACS: 41.20.Cv, 73.21.La, 87.15.A-

Key words: Generalized Coulomb potential, self-polarization potential, quantum dot, hybrid solvation model, Poisson equation.

1 Introduction

In this paper, we are concerned with the calculation of the generalized Coulomb potential energy V_c between two particles inside or outside a dielectric object with the coordinates \mathbf{r} and \mathbf{r}_s , and the charges e and e_s , respectively, which can be evaluated through $V_c(\mathbf{r}, \mathbf{r}_s) = e\Phi(\mathbf{r}, \mathbf{r}_s)$, where $\Phi(\mathbf{r}, \mathbf{r}_s)$ is the electrostatic potential that verifies the Poisson equation

$$\nabla \cdot \varepsilon(\mathbf{r}) \nabla \Phi(\mathbf{r}, \mathbf{r}_s) = -4\pi e_s \delta(\mathbf{r} - \mathbf{r}_s). \quad (1.1)$$

*Corresponding author. *Email addresses:* chfxue@gmail.com (C. Xue), shaodeng@uncc.edu (S. Deng)

Here, $\varepsilon(\mathbf{r})$ is the spatially dependent dielectric function, and $\delta(\dots)$ is the Dirac delta function. Two representative applications of such a problem include the calculation of self-polarization energies of quantum dots (QDs) with finite confinement barriers [1–3], and the calculation of electrostatic interactions in the so-called hybrid explicit/implicit solvation models for treating electrostatic interactions in biomolecular simulations [4], in which the bio-macromolecule together with the solvent molecules in closest proximity of the biomolecule are modeled explicitly with assigned partial charges embedded in a dielectric cavity, and outside the cavity, the solvent is treated implicitly as a dissimilar dielectric continuum.

The three-dimensional solution of the Poisson equation (1.1), even assuming the spherical or spheroidal geometry and only the radial dependence for $\varepsilon(\mathbf{r})$, is quite complicated to find since Eq. (1.1) is a second-order differential equation with a variable, spatially dependent coefficient. Therefore, for simplicity, in most theoretical studies of the underlying applications, macroscopic dielectric constants ε_i and ε_o are assigned for the object (a QD or the dielectric cavity in a hybrid solvation model) and the surrounding medium (the QD matrix or the implicit solvent in the hybrid solvation model), respectively, leading to a sharp jump in the dielectric constant at the object surface. In this case, it is well-known from classical electromagnetism that the presence of a charged particle inside the dielectric object polarizes the surrounding dissimilar dielectric medium, which consequently induces charges at the object surface that have the same or opposite sign as the source charge if the dielectric constant inside the object is higher (the typical situation for QDs) or lower (the typical situation for hybrid solvation models) than that outside. In turn, a new potential energy, usually called the self-polarization energy, arises due to the mutual interaction between the source and its own induced charges.

For the above step-like dielectric model, analytical solutions of the generalized Coulomb and self-polarization potential energies exist for both the spherical and the spheroidal geometries, but unfortunately, there are a few disadvantages of this simple model as well. By construction, all the induced charges will be localized at the object surface of zero width so that both the real and the induced charges can coincide at the same location, giving rise to a self-polarization energy that diverges at the object surface. Besides, the sharp transition from ε_i to ε_o in the dielectric constant at the object surface is clearly unphysical due to interdiffusion between the object and the surrounding medium.

For the spherical geometry, several solutions have been proposed to overcome the inherent mathematical divergence of the step-like dielectric model, including the regularization method [5, 6] (which can be applied to the spheroidal geometry as well), and a more rigorous three-layer dielectric model proposed by Bolcatto and Proetto [3, 7] in which the step-like dielectric function is replaced by a continuous radial dielectric function $\varepsilon(r)$ that changes smoothly from the object value ε_i to the medium value ε_o within a thin translation layer around the object surface. As a direct consequence of such a three-layer model, the induced charges are spread along the translation layer and the mathematical divergence in the self-polarization energy disappears. In fact, Bolcatto *et al.* actually developed a numerical method for the generalized Coulomb and self-polarization

potential energies corresponding to general three-layer dielectric models. However, as the numerical nature of their approach requires the discretization of the continuous dielectric function $\epsilon(r)$ into a multi-step (piecewise constant) one within the translation layer, new numerical divergence is encountered [8]. Recently, a novel three-layer dielectric model that employs a special dielectric permittivity profile for the translation layer and thus allows an analytical series solution of the Poisson equation was proposed [9]. Furthermore, by utilizing this novel three-layer dielectric model, a robust numerical method for general three-layer dielectric models was developed [10], which can completely eliminate the potential numerical divergence of the Bolcatto-Proetto's method, and give convergent results as the number of steps used to discretize the translation layer goes to infinity.

It should be emphasized that, the idea of using a distance-dependent dielectric function such as that in a three-layer dielectric model is definitely not new in biomolecular simulations, since, for instance, it has been widely used in different ways in the so-called implicit solvation models [11, 12]. Unlike the hybrid solvation models [4] mentioned above, implicit solvation models treat the whole solvent outside the macromolecule as a continuous dielectric medium. On the other hand, like the hybrid solvation models, most implicit models treat the continuous implicit solvent as a homogeneous, isotropic medium characterized by a scalar, static dielectric constant, which again is clearly a gross oversimplification and leads to some numerical difficulties. Many different methods have been proposed to overcome this simplification; among those to the interest of the present paper is a class of methods based on the use of distance-dependent dielectric functions, including a linear or quadratic form of the dielectric function [13–15], and more importantly, several sigmoidal forms of dielectric functions [16–19]. In particular, the sigmoidal forms of dielectric functions have been widely used in implicit solvent models for various biomolecular simulations [18–22]. However, using these distance-dependent dielectric functions, how to efficiently obtain an accurate solution to the Poisson or Poisson-Boltzmann equation is a great challenge. Either, the equation needs to be solved numerically at every simulation time step by methods such as finite difference and finite element methods, which, depending on the system size and the solute shape, may become more computationally intensive than standard explicit all-atom solvent simulations. Or, some approximation to the Poisson-Boltzmann equation such as the Generalized Born (GB) model [23, 24] has to be used, which is itself imperfect in, for example, being not easy to obtain accurate estimation of the effective Born radius, a critical parameter for the GB model.

In studying QDs, although state-of-the-art technologies allow to grow QDs of different shape and size [25], most of theoretical and experimental investigations in this field are devoted to QDs of spherical shape. However, it has been shown that small change in external shape of QDs strongly influences energy spectrum and other characteristics of such semiconductor structures [26–29]. Moreover, from geometrical point of view the need to consider spheroidal QDs is actually due to unavoidable small deviations from spherical shape because of deformations during QD growth. On the other hand, in hy-

brid solvation models in biomolecular simulations, although the spherical geometry has often been used to take advantage of the existing analytical solution, for non-spherical bio-macromolecules such as certain globular proteins and other elongated biopolymers like actin and DNA, from computational point of view this treatment may be inefficient, and rather, it may be more beneficial to adopt spheroidal cavities that can conform closely to the irregular shapes of the biomolecules.

For these reasons, the goal of the present paper is to extend the robust numerical method for general three-layer dielectric models from the spherical geometry to the prolate/oblate spheroidal geometries. It should be pointed out, however, that the results obtained in this paper for the spheroidal geometry can then be extended, in essence, to one of the most general three-dimensional systems in which the Laplace equation is separable [30], the triaxial ellipsoidal geometry [31–35]. This extension may be needed since, for example, realistic quantum dots might be neither perfect spheres nor perfect spheroids. The paper is particularly organized as follows. In Section 2, we present the numerical method for general three-layer dielectric models. Then how to extend the results to the oblate spheroidal geometry is briefly discussed in Section 3. Numerical examples are next presented in Section 4, and some concluding remarks are finally given in Section 5. In addition, in Appendixes A and B, we summarily review the analytical series solutions for the step-like and the novel three-layer dielectric models for the prolate spheroidal geometry in order for the paper to be self-contained.

2 Numerical method for general three-layer dielectric models

First of all, in this paper the prolate spheroidal coordinates (ζ, η, ϕ) are defined in terms of the Cartesian ones (x, y, z) as follows:

$$x = \frac{a}{2} \sqrt{(\zeta^2 - 1)(1 - \eta^2)} \cos \phi, \quad y = \frac{a}{2} \sqrt{(\zeta^2 - 1)(1 - \eta^2)} \sin \phi, \quad z = \frac{a}{2} \zeta \eta,$$

where a is the interfocal distance of a prolate spheroid, $\zeta \in [1, \infty)$ is the radial variable, $\eta \in [-1, 1]$ is the angular variable, and $\phi \in [0, 2\pi]$ is the azimuthal variable, respectively. Note that the surface of constant ζ is a prolate spheroid with the same interfocal distance (The surface of $\zeta = 1$ corresponds to the line between the two foci). Also note that here the z -axis is designated as the pole of the prolate spheroidal coordinate system.

As mentioned earlier, the Poisson equation (1.1) with the prolate spheroidal geometry can be solved analytically if $\varepsilon(\mathbf{r})$ assumes the step-like model [36, 37] (see Appendix A). The major problem of employing this simple step-like model and the corresponding analytical solution to calculate the self-polarization energy lies in the fact that it diverges at the surface $\zeta = \zeta_b$ of the spheroidal object. In order to remove both the mathematical singularity of the self-polarization energy and the unphysical assumption of the sharp transition in the dielectric constant at this surface, an intuitive way is to introduce a thin translation layer of finite ζ -dependent width, say 2δ , centered at $\zeta = \zeta_b$ with a continuous radial dielectric profile, say $\varepsilon(\zeta)$, separating the two dielectric continua, leading to

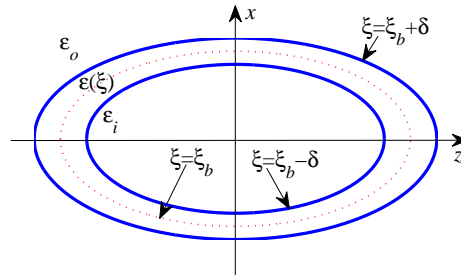


Figure 1: Schematic illustration of a three-layer dielectric model: The inner layer ($\zeta \leq \zeta_b - \delta$) has a dielectric constant of ε_i , while the outer layer ($\zeta \geq \zeta_b + \delta$) has a dielectric constant of ε_o . The intermediate translation layer ($\zeta_b - \delta < \zeta < \zeta_b + \delta$) assumes a continuous dielectric permittivity profile $\varepsilon(\zeta)$ that connects ε_i and ε_o .

a three-layer dielectric model, as shown in Fig. 1. For the inner layer of $\zeta \leq \zeta_b - \delta$ (well inside the object), the dielectric constant takes the value ε_i , while for the outer layer of $\zeta \geq \zeta_b + \delta$ (well outside the object), the dielectric constant takes the value ε_o . Between them, for the intermediate translation layer of $\zeta_b - \delta < \zeta < \zeta_b + \delta$, one can choose any analytical and physically plausible continuous profile for $\varepsilon(\zeta)$ to connect these two extreme values. Two natural choices of $\varepsilon(\zeta)$ include the linear profile defined by

$$\varepsilon(\zeta) = \begin{cases} \varepsilon_i, & \text{if } \zeta \leq \zeta_I, \\ \frac{\varepsilon_i + \varepsilon_o}{2} + \frac{\varepsilon_i - \varepsilon_o}{2\delta} (\zeta_b - \zeta), & \text{if } \zeta_I < \zeta < \zeta_O, \\ \varepsilon_o, & \text{if } \zeta \geq \zeta_O, \end{cases} \quad (2.1)$$

and the cosine-like profile given by

$$\varepsilon(\zeta) = \begin{cases} \varepsilon_i, & \text{if } \zeta \leq \zeta_I, \\ \frac{\varepsilon_i + \varepsilon_o}{2} + \frac{\varepsilon_i - \varepsilon_o}{2} \cos\left(\frac{\zeta - \zeta_I}{2\delta} \pi\right), & \text{if } \zeta_I < \zeta < \zeta_O, \\ \varepsilon_o, & \text{if } \zeta \geq \zeta_O, \end{cases} \quad (2.2)$$

respectively, where $\zeta_I = \zeta_b - \delta$ and $\zeta_O = \zeta_b + \delta$ represent the inner and the outer boundaries (edges) of the intermediate translation layer, respectively.

As indicated before, for a general dielectric permittivity profile $\varepsilon(\zeta)$, it may be infeasible to find the analytical solution of Eq. (1.1) since it is a second-order differential equation with a variable coefficient. When the permittivity assumes a three-layer model with a smooth dielectric profile for the translation layer, by following a procedure as described in [9, 38, 39] for finding the analytical solution to the Poisson equation with the spherical geometry, in principle it may be possible to obtain the analytical solution of Eq. (1.1) with the spheroidal geometry as well. However, inevitably the underlying procedure shall be quite complicated and inefficient for computations because it will involve the solution of a system of some auxiliary second-order differential equations with variable coefficients.

The Poisson equation (1.1) corresponding to a general three-layer dielectric model could also be solved numerically by a procedure similar to that proposed in [3] for calculating self-polarization energies of spherical QDs. First, the translation layer is subdivided into $L-1$ ($L \geq 2$) small regions, and in each of them the select dielectric function $\varepsilon(\xi)$ is approximated by a *constant* value such as the mean value of the dielectric function in that region. As the result, the original Poisson equation with a continuous dielectric function reduces to one for layered dielectric prolate spheroids. By exploiting the analytical solution of the step-like model [36, 37], the solution of the latter could be found in the same manner as for layered spheres [3, 8, 38, 40, 41]. Indeed, this idea or similar has been used to calculate the potential distribution in a layered anisotropic spheroidal volume conductor [42]. However, this approach has the same fundamental limitation: as its numerical nature requires the discretization of a continuous radial dielectric function $\varepsilon(\xi)$ into a piecewise constant one within the translation layer, new numerical divergence emerges. No matter how many small regions are used to discretize the translation layer, the ultimate effect of this multi-step approximation of a continuous radial dielectric profile $\varepsilon(\xi)$ is to approximate a continuous self-polarization energy profile by one with divergence at every step edge. We thus believe that for a general three-layer dielectric model, this procedure does not necessarily converge, let alone is able to recover the exact solution of the corresponding Poisson equation when L goes to infinity.

Therefore, in this paper we would like to develop a robust numerical method for general three-layer dielectric models by exploiting the analytical solution of the following three-layer dielectric model [43]

$$\varepsilon(\xi) = \begin{cases} \varepsilon_i, & \text{if } \xi \leq \xi_I, \\ \left[\alpha + \frac{\beta}{2} \ln \left(\frac{\xi+1}{\xi-1} \right) \right]^2, & \text{if } \xi_I < \xi < \xi_O, \\ \varepsilon_o, & \text{if } \xi \geq \xi_O, \end{cases} \quad (2.3)$$

where

$$\alpha = \frac{c\sqrt{\varepsilon_o} - d\sqrt{\varepsilon_i}}{c-d}, \quad \beta = \frac{\sqrt{\varepsilon_i} - \sqrt{\varepsilon_o}}{c-d},$$

with

$$c = \frac{1}{2} \ln \left(\frac{\xi_I+1}{\xi_I-1} \right), \quad d = \frac{1}{2} \ln \left(\frac{\xi_O+1}{\xi_O-1} \right).$$

For convenience, here and in the sequel, the dielectric permittivity profile in the translation layer given by (2.3) is referred to as the *quasi-harmonic* profile since, although originally it was constructed through two harmonic functions $P_0^0(\xi) \equiv 1$ and $Q_0^0(\xi) = \frac{1}{2} \ln((\xi+1)/(\xi-1))$, it is not harmonic by itself. Note that in this paper $P_n^m(\dots)$ and $Q_n^m(\dots)$ represent the associated Legendre functions of the first and second kinds. The three three-layer dielectric models mentioned so far together with the step-like model are illustrated in Fig. 2. As can be seen, like the linear profile, the derivative of the quasi-harmonic dielectric profile is discontinuous at both edges of the translation layer, whereas the cosine-like dielectric profile is smooth at the same locations.

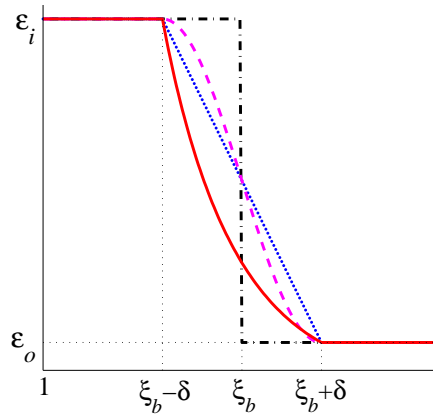


Figure 2: Illustration of several dielectric models for the translation layer between $\xi_b - \delta$ and $\xi_b + \delta$, assuming $\epsilon_i > \epsilon_o$. Dot-dashed line, the step-like model; dotted line, the linear model; dashed line, the cosine-like model; and solid line, the quasi-harmonic model.

The analytical solution to the Poisson equation (1.1) corresponding to this quasi-harmonic dielectric model is easy to find [43] (see Appendix B), based on which and motivated from Bolcatto *et al.*'s work [3, 7], we shall develop a numerical method for solving the Poisson equation (1.1) for general three-layer dielectric models. The basic idea is still simple. The dielectric translation layer, $\xi_b - \delta < \xi < \xi_b + \delta$, is first subdivided into multiple, say $L - 1$, small regions. Then, in each of them the select continuous radial dielectric function $\epsilon(\xi)$ is approximated by a quasi-harmonic one $\epsilon_l(\xi)$ of the form (2.3). In this way the original continuous dielectric function is approximated by a piecewise smooth but yet continuous one. Next, in each region the series solution of the Poisson equation is written in terms of the associated Legendre functions. Finally, by following the spirit of [10, 38, 40], namely, by using a procedure in analogy to the analysis of transmission lines, we obtain recursive formulas for calculating those expansion coefficients in the series solutions. This numerical method completely eliminates the numerical divergence in the self-polarization energy that occurs if the dielectric function in each region is approximated simply by a constant value [3], and thus shall be able to recover the exact solution of the corresponding Poisson equation as $L \rightarrow \infty$.

2.1 Approximation of three-layer dielectric models and notations

As being pointed out already, the translation layer, $\xi_b - \delta < \xi < \xi_b + \delta$, is subdivided into $L - 1$ regions, $[\xi_{l-1}, \xi_l]$, $l = 1, \dots, L - 1$, with $\xi_0 = \xi_b - \delta$ and $\xi_{L-1} = \xi_b + \delta$, as shown in Fig. 3. For convenience, we also set $\xi_{-1} = 1$ and $\xi_L = \infty$. So, including $[1, \xi_0]$ and $[\xi_{L-1}, \infty)$, in total there are $L + 1$ regions, or equivalently, L steps.

For each index $l = -1, 0, \dots, L$, we denote by e_l the dielectric constant at $\xi = \xi_l$, namely, $e_l = \epsilon(\xi_l)$. Note that $e_{-1} = e_0 = \epsilon_i$ and $e_{L-1} = e_L = \epsilon_o$. In each region $[\xi_{l-1}, \xi_l]$, $l = 0, 1, \dots, L$, the

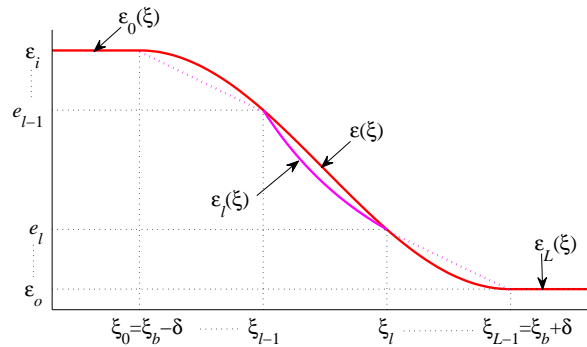


Figure 3: Illustration of the L -step approximation of a three-layer dielectric model. The dielectric constants of the inner layer, $[1, \xi_b - \delta]$, and the outer layer, $[\xi_b + \delta, \infty)$, are $\varepsilon_0(\xi) \equiv \varepsilon_i$ and $\varepsilon_L(\xi) \equiv \varepsilon_o$, respectively. The intermediate translation layer, $[\xi_b - \delta, \xi_b + \delta]$, is subdivided into $L - 1$ regions, the dielectric permittivity in each of them, say $[\xi_{l-1}, \xi_l]$, being approximated by $\varepsilon_l(\xi)$ of the form (2.3). Note that $\xi_0 = \xi_b - \delta$ and $\xi_{L-1} = \xi_b + \delta$. Also, for convenience, we set $\xi_{-1} = 1$ and $\xi_L = \infty$, respectively.

select continuous dielectric function $\varepsilon(\xi)$ is approximated by a quasi-harmonic dielectric function $\varepsilon_l(\xi)$ of the form (2.3) that connects e_{l-1} and e_l , i.e.,

$$\varepsilon_l(\xi) = \left[\alpha_l + \frac{\beta_l}{2} \ln \left(\frac{\xi + 1}{\xi - 1} \right) \right]^2, \quad \xi_{l-1} \leq \xi \leq \xi_l, \quad l = 0, 1, \dots, L,$$

where

$$\alpha_l = \frac{c_l \sqrt{e_l} - d_l \sqrt{e_{l-1}}}{c_l - d_l}, \quad \beta_l = \frac{\sqrt{e_{l-1}} - \sqrt{e_l}}{c_l - d_l},$$

with

$$c_l = \frac{1}{2} \ln \left(\frac{\xi_{l-1} + 1}{\xi_{l-1} - 1} \right), \quad d_l = \frac{1}{2} \ln \left(\frac{\xi_l + 1}{\xi_l - 1} \right).$$

Note that $\varepsilon_0(\xi) \equiv \varepsilon_i, \varepsilon_L(\xi) \equiv \varepsilon_o, \alpha_0 = \sqrt{e_i}, \alpha_L = \sqrt{e_o}$, and $\beta_0 = \beta_L = 0$. Fig. 4 shows the L -step approximations of the linear and the cosine-like dielectric models by quasi-harmonic dielectric functions with $L = 3$ and $L = 5$, respectively.

In what follows, for $n = 0, 1, \dots$, and $m = 0, 1, \dots, n$, we let

$$u_{mn}(\xi) = \frac{P_n^m(\xi)}{Q_n^m(\xi)}, \quad v_{mn}(\xi) = \frac{Q_n^m(\xi)}{P_n^m(\xi)},$$

and define

$$\gamma_{mn,l} = u_{mn}(\xi_{l-1})v_{mn}(\xi_l), \quad l = 0, 1, \dots, L.$$

Note that $\gamma_{mn,0} = \gamma_{mn,L} = 0$ since $Q_n^m(1) = \infty$ and $P_n^m(\infty) = \infty$. And more generally, we let

$$\gamma_{mn,ij} = u_{mn}(\xi_{i-1})v_{mn}(\xi_j), \quad 0 \leq i \leq j \leq L.$$

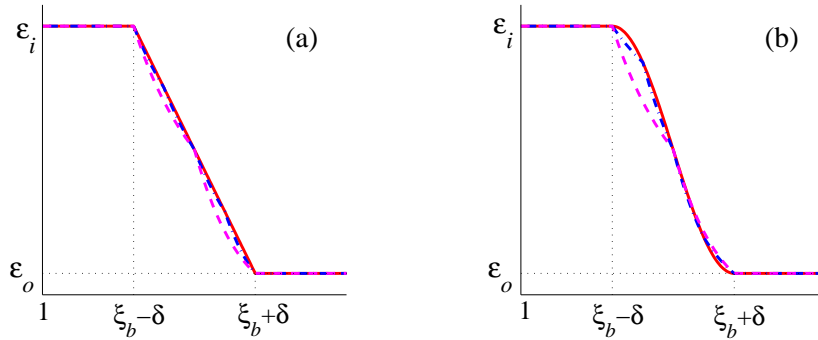


Figure 4: Illustration of the L -step approximations of the linear and the cosine-like models by quasi-harmonic dielectric functions with $L=3$ and $L=5$, respectively, assuming $\epsilon_i > \epsilon_o$. (a) The linear model, and (b) the cosine-like model. Solid line, the original linear or cosine-like dielectric model; dashed line, the 3-step approximation; and dot-dashed line, the 5-step approximation.

Also, without loss of generality, in this paper we assume that a point charge e_s is always located at a point $\mathbf{r}_s = (\xi_s, \eta_s, \phi_s = 0)$ in the xz -plane, and for convenience, throughout the paper we use the following shorthand notations.

$$\begin{aligned} \mathcal{H}_{mn} &= 2(2n+1)(2-\delta_{m0})(-1)^m \left[\frac{(n-m)!}{(n+m)!} \right]^2, \\ \tilde{\mathcal{H}}_{mn} &= \mathcal{H}_{mn} P_n^m(\eta_s), \\ \mathcal{H}_{mn}^P &= \tilde{\mathcal{H}}_{mn} P_n^m(\xi_s), \\ \mathcal{H}_{mn}^Q &= \tilde{\mathcal{H}}_{mn} Q_n^m(\xi_s), \\ \bar{P}_n^m(\xi) &= (n-m+1)P_{n+1}^m(\xi)/P_n^m(\xi) - (n+1)\xi, \\ \bar{Q}_n^m(\xi) &= (n-m+1)Q_{n+1}^m(\xi)/Q_n^m(\xi) - (n+1)\xi, \end{aligned}$$

where δ_{m0} is the Kronecker delta.

2.2 Case I – The source charge is in the region 0: $\xi_s \in [1, \xi_0]$

In this paper, for each index l with $0 \leq l \leq L$, we denote by $\Phi_l(\mathbf{r}, \mathbf{r}_s)$ the potential at the point \mathbf{r} in the region l , $[\xi_{l-1}, \xi_l]$, generated by a point charge e_s with the coordinate \mathbf{r}_s . When e_s is located inside the region 0, the approximation of the Poisson equation (1.1) becomes

$$\Delta \Phi_L(\mathbf{r}, \mathbf{r}_s) = 0, \tag{2.4a}$$

$$\nabla \cdot \epsilon_l(\xi) \nabla \Phi_l(\mathbf{r}, \mathbf{r}_s) = 0, \quad l = 1, \dots, L-1, \tag{2.4b}$$

$$\nabla \cdot \epsilon_0 \nabla \Phi_0(\mathbf{r}, \mathbf{r}_s) = -4\pi e_s \delta(\mathbf{r} - \mathbf{r}_s). \tag{2.4c}$$

At the same time, across each interface $\xi = \xi_{l-1}, l = 1, \dots, L$, the following conditions hold.

$$\Phi_{l-1}|_{\xi=\xi_{l-1}^-} = \Phi_l|_{\xi=\xi_{l-1}^+}, \quad \left. \frac{\partial \Phi_{l-1}}{\partial \xi} \right|_{\xi=\xi_{l-1}^-} = \left. \frac{\partial \Phi_l}{\partial \xi} \right|_{\xi=\xi_{l-1}^+}. \tag{2.5}$$

To solve Eq. (2.4), motivated from Eq. (B.1), first we write its solution in the form

$$\Phi_L(\mathbf{r}, \mathbf{r}_s) = \frac{e_s}{\sqrt{e_0 e_L} a} \sum_{n=0}^{\infty} \sum_{m=0}^n \mathcal{H}_{mn}^P D_{mn}^L Q_n^m(\xi) Y_n^m(\phi, \eta), \tag{2.6a}$$

$$\Phi_l(\mathbf{r}, \mathbf{r}_s) = \frac{e_s}{\sqrt{e_0 e_l}(\xi) a} \sum_{n=0}^{\infty} \sum_{m=0}^n \mathcal{H}_{mn}^P [v_{mn}(\xi_l) C_{mn}^l P_n^m(\xi) + D_{mn}^l Q_n^m(\xi)] Y_n^m(\phi, \eta), \tag{2.6b}$$

$$\Phi_0(\mathbf{r}, \mathbf{r}_s) = \frac{e_s}{e_0 |\mathbf{r} - \mathbf{r}_s|} + \frac{e_s}{e_0 a} \sum_{n=0}^{\infty} \sum_{m=0}^n \mathcal{H}_{mn}^P v_{mn}(\xi_0) C_{mn}^0 P_n^m(\xi) Y_n^m(\phi, \eta), \tag{2.6c}$$

where l in Eq. (2.6b) takes values between 1 and $L-1$, and $Y_n^m(\phi, \eta)$ represents the spheroidal surface harmonic given by

$$Y_n^m(\phi, \eta) = \cos(m\phi) P_n^m(\eta).$$

Also, here and in the sequel, any superscript other than 2 simply indicates a super index rather than a mathematical power.

In order to determine the constant expansion coefficients $C_{mn}^l, l = 0, 1, \dots, L-1$, and $D_{mn}^l, l = 1, \dots, L$, relations for these coefficients are first obtained from the interface conditions (2.5), together with the orthogonality of $\cos(m\phi)$ and that of $P_n^m(\dots)$, as well as the widely-known expansion of the reciprocal distance in the prolate spheroidal coordinates [30, 44, 45], namely,

$$\frac{1}{|\mathbf{r} - \mathbf{r}_s|} = \begin{cases} \frac{1}{a} \sum_{n=0}^{\infty} \sum_{m=0}^n \mathcal{H}_{mn}^P Q_n^m(\xi) Y_n^m(\phi, \eta), & \text{if } \xi \geq \xi_s, \\ \frac{1}{a} \sum_{n=0}^{\infty} \sum_{m=0}^n \mathcal{H}_{mn}^Q P_n^m(\xi) Y_n^m(\phi, \eta), & \text{if } \xi \leq \xi_s. \end{cases} \tag{2.7}$$

Omitting all details, for $l = 1, \dots, L, n = 0, 1, \dots$, and $m = 0, 1, \dots, n$, we get

$$\gamma_{mn,l} C_{mn}^l + D_{mn}^l = C_{mn}^{l-1} + D_{mn}^{l-1}, \tag{2.8a}$$

$$a_{mn,l} \gamma_{mn,l} C_{mn}^l + b_{mn,l} D_{mn}^l = c_{mn,l} C_{mn}^{l-1} + d_{mn,l} D_{mn}^{l-1}, \tag{2.8b}$$

where $D_{mn}^0 = 1$ and $C_{mn}^L = 0$, and

$$\begin{aligned} a_{mn,l} &= \sqrt{e_{l-1}} \bar{P}_n^m(\xi_{l-1}) + \beta_l, \\ b_{mn,l} &= \sqrt{e_{l-1}} \bar{Q}_n^m(\xi_{l-1}) + \beta_l, \\ c_{mn,l} &= \sqrt{e_{l-1}} \bar{P}_n^m(\xi_{l-1}) + \beta_{l-1}, \\ d_{mn,l} &= \sqrt{e_{l-1}} \bar{Q}_n^m(\xi_{l-1}) + \beta_{l-1}. \end{aligned}$$

Next, we follow the spirit of [38, 40] to seek the analytical solution of the expansion coefficients in some recursive way. Specifically, in analogy to the analysis of transmission lines, we call each term of the sum in Eq. (2.6b) corresponding to a pair of indices n and m , a mode of the potential. Each mode has two functions of ξ , of which the one with $P_n^m(\xi)$ might be called a 'static wave' propagating towards the center, while the other with $Q_n^m(\xi)$ is propagating towards infinity. Thus, at each interface we define static reflection and transmission coefficients as ratios of the two static waves at each side of the interface, relations for these coefficients being obtained from the interface relations (2.8). In particular, at the $-$ side of each interface, say $\xi = \xi_{l-1}$, we denote by T_{mn}^{l-1} the transmission coefficient associated to the interface $\xi = \xi_{l-1}$, defined as the ratio of the transmitted and the reflected waves, namely,

$$T_{mn}^{l-1} \equiv \frac{v_{mn}(\xi_{l-1})C_{mn}^{l-1}P_n^m(\xi_{l-1})}{D_{mn}^{l-1}Q_n^m(\xi_{l-1})} = \frac{C_{mn}^{l-1}}{D_{mn}^{l-1}}.$$

Note that $T_{mn}^L = 0$ since $C_{mn}^L = 0$, and $T_{mn}^0 = C_{mn}^0$ since $D_{mn}^0 = 1$.

Then, to derive a recursive formula for the transmission coefficient T_{mn}^{l-1} , the system (2.8) is rewritten in the form

$$\begin{pmatrix} D_{mn}^l \\ C_{mn}^{l-1} \end{pmatrix} = \begin{pmatrix} R_{mn,l} & T_{mn,l} \\ T_{mn,l} & R_{mn,l} \end{pmatrix} \begin{pmatrix} \gamma_{mn,l} & 0 \\ 0 & 1 \end{pmatrix} \begin{pmatrix} C_{mn}^l \\ D_{mn}^{l-1} \end{pmatrix}, \quad (2.9)$$

where $R_{mn,l}$ and $T_{mn,l}$, identified as the interface parameters associated to the interface $\xi = \xi_{l-1}$, are given by

$$\begin{aligned} R_{mn,l} &= \frac{1}{\Delta_{mn,l}}(\beta_{l-1} - \beta_l), \\ T_{mn,l} &= \frac{\sqrt{e_{l-1}}}{\Delta_{mn,l}} \left(\bar{Q}_n^m(\xi_{l-1}) - \bar{P}_n^m(\xi_{l-1}) \right), \\ \Delta_{mn,l} &= \sqrt{e_{l-1}} \left(\bar{Q}_n^m(\xi_{l-1}) - \bar{P}_n^m(\xi_{l-1}) \right) - (\beta_{l-1} - \beta_l). \end{aligned}$$

Now let the transmission coefficient at the $-$ side of the next interface $\xi = \xi_l$ be denoted by T_{mn}^l , which equals to C_{mn}^l / D_{mn}^l . Then substituting $C_{mn}^l = T_{mn}^l D_{mn}^l$ in the system (2.9), we get the following relation between the transmission coefficients T_{mn}^{l-1} and T_{mn}^l

$$T_{mn}^{l-1} = R_{mn,l} + \frac{T_{mn,l}^2 T_{mn}^l \gamma_{mn,l}}{1 - R_{mn,l} T_{mn}^l \gamma_{mn,l}}. \quad (2.10)$$

This gives us the transformation formula for the total transmission coefficient from the interface $\xi = \xi_l$ to the interface $\xi = \xi_{l-1}$. Thus, the transmission coefficient T_{mn}^{l-1} can be obtained from the knowledge of two interface parameters $R_{mn,l}$ and $T_{mn,l}$ associated to the interface $\xi = \xi_{l-1}$ plus the transmission coefficient T_{mn}^l associated to the next interface $\xi = \xi_l$. Similarly, T_{mn}^l can be obtained from a similar expression in terms of the interface

parameters $R_{mn,l+1}$ and $T_{mn,l+1}$ at the interface $\xi = \xi_l$ plus the transmission coefficient T_{mn}^{l+1} at the next interface $\xi = \xi_{l+1}$. Continuing this, we come finally to the outermost interface $\xi = \xi_{L-1}$, at which the total transmission coefficient equals the transmission coefficient of that interface. This is owing to the fact that, after this interface, there only exist waves that propagate towards infinity, implying that only $D_{mn}^L \neq 0$. As $C_{mn}^L = 0$, also $T_{mn}^L = 0$, this gives $T_{mn}^{L-1} = R_{mn,L}$. Therefore, a recursive expression for T_{mn}^{l-1} can be obtained in this manner from the knowledge of all interface parameters associated to the interfaces $\xi_{L-1}, \xi_{L-2}, \dots, \xi_{l-1}$.

Finally, by solving the system (2.8), we obtain a recursive formula for the expansion coefficients C_{mn}^l and $D_{mn}^l, l=0,1,\dots,L$, in (2.6) using the transmission coefficients, namely,

$$D_{mn}^l = \frac{T_{mn,l}}{1 - R_{mn,l}T_{mn}^l\gamma_{mn,l}} D_{mn}^{l-1}, \tag{2.11a}$$

$$C_{mn}^l = T_{mn}^l D_{mn}^l, \tag{2.11b}$$

in which $D_{mn}^0 = 1$, and $C_{mn}^0 = T_{mn}^0$.

2.3 Case II – The source charge is in the region L: $\xi_s \in [\xi_{L-1}, \infty)$

When the source charge e_s is located inside the region L, the approximation of the Poisson equation (1.1) becomes

$$\nabla \cdot e_L \nabla \Phi_L(\mathbf{r}, \mathbf{r}_s) = -4\pi e_s \delta(\mathbf{r} - \mathbf{r}_s), \tag{2.12a}$$

$$\nabla \cdot \epsilon_l(\xi) \nabla \Phi_l(\mathbf{r}, \mathbf{r}_s) = 0, \quad l = 1, \dots, L-1, \tag{2.12b}$$

$$\Delta \Phi_0(\mathbf{r}, \mathbf{r}_s) = 0. \tag{2.12c}$$

To solve Eq. (2.12), motivated from Eq. (B.2), first we write its solution in the form

$$\Phi_L(\mathbf{r}, \mathbf{r}_s) = \frac{e_s}{e_L |\mathbf{r} - \mathbf{r}_s|} + \frac{e_s}{e_L a} \sum_{n=0}^{\infty} \sum_{m=0}^n \mathcal{H}_{mn}^Q u_{mn}(\xi_{L-1}) D_{mn}^L Q_n^m(\xi) Y_n^m(\phi, \eta), \tag{2.13a}$$

$$\Phi_l(\mathbf{r}, \mathbf{r}_s) = \frac{e_s}{\sqrt{e_L \epsilon_l(\xi)} a} \sum_{n=0}^{\infty} \sum_{m=0}^n \mathcal{H}_{mn}^Q [C_{mn}^l P_n^m(\xi) + u_{mn}(\xi_{l-1}) D_{mn}^l Q_n^m(\xi)] Y_n^m(\phi, \eta), \tag{2.13b}$$

$$\Phi_0(\mathbf{r}, \mathbf{r}_s) = \frac{e_s}{\sqrt{e_L \epsilon_0} a} \sum_{n=0}^{\infty} \sum_{m=0}^n \mathcal{H}_{mn}^Q C_{mn}^0 P_n^m(\xi) Y_n^m(\phi, \eta), \tag{2.13c}$$

where l in Eq. (2.13b) takes values between 1 and $L-1$.

Similarly, relations for the expansion coefficients $C_{mn}^l, l=0,1,\dots,L-1$, and $D_{mn}^l, l=1,\dots,L$, are obtained from the interface conditions (2.5). Passing all details, for $l=1,\dots,L, n=0,1,\dots$, and $m=0,1,\dots,n$, we get

$$C_{mn}^l + D_{mn}^l = C_{mn}^{l-1} + \gamma_{mn,l-1} D_{mn}^{l-1}, \tag{2.14a}$$

$$a_{mn,l} C_{mn}^l + b_{mn,l} D_{mn}^l = c_{mn,l} C_{mn}^{l-1} + d_{mn,l} \gamma_{mn,l-1} D_{mn}^{l-1}, \tag{2.14b}$$

where $C_{mn}^L = 1$ and $D_{mn}^0 = 0$.

Now, at the + side of each interface, say $\zeta = \zeta_{l-1}$, we denote by R_{mn}^{l-1} the reflection coefficient associated to the interface $\zeta = \zeta_{l-1}$, defined as the ratio of the reflected and the transmitted waves, namely,

$$R_{mn}^{l-1} \equiv \frac{u_{mn}(\zeta_{l-1})D_{mn}^l Q_n^m(\zeta_{l-1})}{C_{mn}^l P_n^m(\zeta_{l-1})} = \frac{D_{mn}^l}{C_{mn}^l}.$$

Note that $R_{mn}^{-1} = 0$ since $D_{mn}^0 = 0$, and $R_{mn}^{L-1} = D_{mn}^L$ since $C_{mn}^L = 1$.

In order to derive a recursive formula for the reflection coefficient R_{mn}^{l-1} , the system (2.14) is rewritten in the form

$$\begin{pmatrix} D_{mn}^l \\ C_{mn}^{l-1} \end{pmatrix} = \begin{pmatrix} R_{mn,l} & T_{mn,l} \\ T_{mn,l} & R_{mn,l} \end{pmatrix} \begin{pmatrix} 1 & 0 \\ 0 & \gamma_{mn,l-1} \end{pmatrix} \begin{pmatrix} C_{mn}^l \\ D_{mn}^{l-1} \end{pmatrix}. \quad (2.15)$$

Let the reflection coefficient at the + side of the next interface $\zeta = \zeta_{l-2}$ be denoted by R_{mn}^{l-2} , which equals to $D_{mn}^{l-1}/C_{mn}^{l-1}$. Then substituting $D_{mn}^{l-1} = R_{mn}^{l-2}C_{mn}^{l-1}$ in the system (2.15), we have the following relation between the reflection coefficients R_{mn}^{l-1} and R_{mn}^{l-2}

$$R_{mn}^{l-1} = R_{mn,l} + \frac{T_{mn,l}^2 R_{mn}^{l-2} \gamma_{mn,l-1}}{1 - R_{mn,l} R_{mn}^{l-2} \gamma_{mn,l-1}}. \quad (2.16)$$

This gives us the transformation formula for the total reflection coefficient from the interface $\zeta = \zeta_{l-2}$ to the interface $\zeta = \zeta_{l-1}$. Thus, the reflection coefficient R_{mn}^{l-1} can be obtained from the knowledge of two interface parameters $R_{mn,l}$ and $T_{mn,l}$ associated to the interface $\zeta = \zeta_{l-1}$ plus the reflection coefficient R_{mn}^{l-2} associated to the next interface $\zeta = \zeta_{l-2}$. Likewise, R_{mn}^{l-2} can be obtained from a similar expression in terms of the interface parameters $R_{mn,l-1}$ and $T_{mn,l-1}$ at the interface $\zeta = \zeta_{l-2}$ plus the reflection coefficient R_{mn}^{l-3} at the next interface $\zeta = \zeta_{l-3}$. Continuing this, we come finally to the innermost interface $\zeta = \zeta_0$, at which the total reflection coefficient equals the reflection coefficient of that interface. This is owing to the fact that, after this interface, there only exist waves that propagate towards the center, implying that only $C_{mn}^0 \neq 0$. As $D_{mn}^0 = 0$, also $R_{mn}^{-1} = 0$, this gives $R_{mn}^0 = R_{mn,1}$. Therefore, a recursive expression for R_{mn}^{l-1} can be obtained in this manner from the knowledge of all interface parameters associated to the interfaces $\zeta_0, \zeta_1, \dots, \zeta_{l-1}$.

Finally, by solving the system (2.14), we obtain a recursive formula for the expansion coefficients C_{mn}^l and D_{mn}^l , $l = 0, 1, \dots, L$, in (2.13) using the reflection coefficients, namely,

$$C_{mn}^{l-1} = \frac{T_{mn,l}}{1 - R_{mn,l} R_{mn}^{l-2} \gamma_{mn,l-1}} C_{mn}^l, \quad (2.17a)$$

$$D_{mn}^{l-1} = R_{mn}^{l-2} C_{mn}^{l-1}, \quad (2.17b)$$

in which $C_{mn}^L = 1$, and $D_{mn}^L = R_{mn}^{L-1}$.

2.4 Case III – The charge is in the region k : $\zeta_s \in [\zeta_{k-1}, \zeta_k]$ where $0 < k < L$

When the source charge e_s lies in the region k with $0 < k < L$, the approximation of the Poisson equation (1.1) in that particular region becomes

$$\nabla \cdot \varepsilon_k(\zeta) \nabla \Phi_k(\mathbf{r}, \mathbf{r}_s) = -4\pi e_s \delta(\mathbf{r} - \mathbf{r}_s). \tag{2.18}$$

First, the electrostatic potential satisfying Eq. (2.18) can be written in the general form

$$\Phi_k(\mathbf{r}, \mathbf{r}_s) = \frac{e_s}{\sqrt{\varepsilon_s \varepsilon_k(\zeta)} |\mathbf{r} - \mathbf{r}_s|} + \frac{e_s}{\sqrt{\varepsilon_s \varepsilon_k(\zeta)} a} \sum_{n=0}^{\infty} \sum_{m=0}^n \left(\bar{C}_{mn}^k P_n^m(\zeta) + \bar{D}_{mn}^k Q_n^m(\zeta) \right) Y_n^m(\phi, \eta), \tag{2.19}$$

where $\varepsilon_s = \varepsilon_k(\zeta_s)$, and the two expansion coefficients \bar{C}_{mn}^k and \bar{D}_{mn}^k can be determined from the transmission and the reflection coefficients T_{mn}^k and R_{mn}^{k-1} as described below.

Using the expansion of the reciprocal distance (2.7), on the one hand, at the $-$ side of the interface $\zeta = \zeta_k$, the potential $\Phi_k(\mathbf{r}, \mathbf{r}_s)$ can be rewritten as

$$\Phi_k(\mathbf{r}, \mathbf{r}_s) = \frac{e_s}{\sqrt{\varepsilon_s \varepsilon_k(\zeta)} a} \sum_{n=0}^{\infty} \sum_{m=0}^n \left(\bar{C}_{mn}^k P_n^m(\zeta) + \bar{D}_{mn}^{k*} Q_n^m(\zeta) \right) Y_n^m(\phi, \eta),$$

where $\bar{D}_{mn}^{k*} = \bar{D}_{mn}^k + \mathcal{H}_{mn}^P$. On the other hand, at the $+$ side of the interface $\zeta = \zeta_{k-1}$, it can be rewritten as

$$\Phi_k(\mathbf{r}, \mathbf{r}_s) = \frac{e_s}{\sqrt{\varepsilon_s \varepsilon_k(\zeta)} a} \sum_{n=0}^{\infty} \sum_{m=0}^n \left(\bar{C}_{mn}^{k*} P_n^m(\zeta) + \bar{D}_{mn}^k Q_n^m(\zeta) \right) Y_n^m(\phi, \eta),$$

where $\bar{C}_{mn}^{k*} = \bar{C}_{mn}^k + \mathcal{H}_{mn}^Q$. Thus, by recalling the definitions of T_{mn}^k and R_{mn}^{k-1} , we get

$$T_{mn}^k = u_{mn}(\zeta_k) \times \frac{\bar{C}_{mn}^k}{\bar{D}_{mn}^{k*}}, \tag{2.20a}$$

$$R_{mn}^{k-1} = v_{mn}(\zeta_{k-1}) \times \frac{\bar{D}_{mn}^k}{\bar{C}_{mn}^{k*}}. \tag{2.20b}$$

Solving the system (2.20) for \bar{C}_{mn}^k and \bar{D}_{mn}^k and plugging them in Eq. (2.19) finally give us

$$\begin{aligned} \Phi_k(\mathbf{r}, \mathbf{r}_s) &= \frac{e_s}{\sqrt{\varepsilon_s \varepsilon_k(\zeta)} |\mathbf{r} - \mathbf{r}_s|} + \frac{e_s}{\sqrt{\varepsilon_s \varepsilon_k(\zeta)} a} \\ &\times \sum_{n=0}^{\infty} \sum_{m=0}^n \left[\left(\mathcal{H}_{mn}^Q \gamma_{mn,k} C_{mn}^{k(1)} + \mathcal{H}_{mn}^P v_{mn}(\zeta_k) C_{mn}^{k(2)} \right) P_n^m(\zeta) \right. \\ &\left. + \left(\mathcal{H}_{mn}^Q u_{mn}(\zeta_{k-1}) D_{mn}^{k(1)} + \mathcal{H}_{mn}^P \gamma_{mn,k} D_{mn}^{k(2)} \right) Q_n^m(\zeta) \right] Y_n^m(\phi, \eta), \end{aligned} \tag{2.21}$$

in which the ζ_s -independent expansion coefficients are defined as

$$C_{mn}^{k(2)} = \frac{T_{mn}^k}{1 - R_{mn}^{k-1} T_{mn}^k \gamma_{mn,k}}, \tag{2.22a}$$

$$D_{mn}^{k(1)} = \frac{R_{mn}^{k-1}}{1 - R_{mn}^{k-1} T_{mn}^k \gamma_{mn,k}}, \tag{2.22b}$$

$$C_{mn}^{k(1)} = R_{mn}^{k-1} C_{mn}^{k(2)}, \tag{2.22c}$$

$$D_{mn}^{k(2)} = T_{mn}^k D_{mn}^{k(1)}. \tag{2.22d}$$

Moreover, by using (2.7) again, $\Phi_k(\mathbf{r}, \mathbf{r}_s)$ can be written in a more concise form as

$$\Phi_k(\mathbf{r}, \mathbf{r}_s) = \frac{e_s}{\sqrt{\varepsilon_s \varepsilon_k(\zeta)} a} \sum_{n=0}^{\infty} \sum_{m=0}^n \tilde{\mathcal{H}}_{mn} Y_n^m(\phi, \eta) \times \frac{F_{mn,kk}(\zeta, \zeta_s)}{1 - R_{mn}^{k-1} T_{mn}^k \gamma_{mn,k}}, \tag{2.23}$$

where, assuming that $\zeta_<$ ($\zeta_>$) is the smaller (greater) between ζ and ζ_s ,

$$F_{mn,kk}(\zeta, \zeta_s) = \left[T_{mn}^k v_{mn}(\zeta_k) P_n^m(\zeta_>) + Q_n^m(\zeta_>) \right] \left[P_n^m(\zeta_<) + R_{mn}^{k-1} u_{mn}(\zeta_{k-1}) Q_n^m(\zeta_<) \right].$$

Next, let us consider the electrostatic potential in a general region l with $l \neq k$, in which the approximation of the Poisson equation (1.1) is

$$\nabla \cdot \varepsilon_l(\zeta) \nabla \Phi_l(\mathbf{r}, \mathbf{r}_s) = 0. \tag{2.24}$$

In the case of $0 \leq l < k$, similar to Eq. (2.13b) we write the solution of Eq. (2.24) in the form

$$\Phi_l(\mathbf{r}, \mathbf{r}_s) = \frac{e_s}{\sqrt{\varepsilon_s \varepsilon_l(\zeta)} a} \sum_{n=0}^{\infty} \sum_{m=0}^n \mathcal{H}_{mn}^Q \left[C_{mn}^l P_n^m(\zeta) + u_{mn}(\zeta_{l-1}) D_{mn}^l Q_n^m(\zeta) \right] Y_n^m(\phi, \eta), \tag{2.25}$$

and accordingly rewrite $\Phi_k(\mathbf{r}, \mathbf{r}_s)$ as

$$\Phi_k(\mathbf{r}, \mathbf{r}_s) = \frac{e_s}{\sqrt{\varepsilon_s \varepsilon_k(\zeta)} a} \sum_{n=0}^{\infty} \sum_{m=0}^n \mathcal{H}_{mn}^Q \left[C_{mn}^k P_n^m(\zeta) + u_{mn}(\zeta_{k-1}) D_{mn}^k Q_n^m(\zeta) \right] Y_n^m(\phi, \eta),$$

where

$$C_{mn}^k = 1 + \frac{\bar{C}_{mn}^k}{\mathcal{H}_{mn}^Q}, \quad D_{mn}^k = v_{mn}(\zeta_{k-1}) \times \frac{\bar{D}_{mn}^k}{\mathcal{H}_{mn}^Q}.$$

Then, for $l=k-1, k-2, \dots, 0$, we can calculate C_{mn}^l and D_{mn}^l in Eq. (2.25) using the recursive formula (2.17). Substituting them in Eq. (2.25) and rewriting the result, we get

$$\begin{aligned} \Phi_l(\mathbf{r}, \mathbf{r}_s) = & \frac{e_s}{\sqrt{\varepsilon_s \varepsilon_l(\zeta)} a} \sum_{n=0}^{\infty} \sum_{m=0}^n \left[\left(\mathcal{H}_{mn}^Q C_{mn}^{l(1)} + \mathcal{H}_{mn}^P v_{mn}(\zeta_k) C_{mn}^{l(2)} \right) P_n^m(\zeta) \right. \\ & \left. + \left(\mathcal{H}_{mn}^Q u_{mn}(\zeta_{l-1}) D_{mn}^{l(1)} + \mathcal{H}_{mn}^P \gamma_{mn,lk} D_{mn}^{l(2)} \right) Q_n^m(\zeta) \right] Y_n^m(\phi, \eta), \end{aligned} \tag{2.26}$$

where

$$\begin{aligned} C_{mn}^{l(1)} &= \frac{\tilde{C}_{mn}^l}{1 - R_{mn}^{k-1} T_{mn}^k \gamma_{mn,k}}, & C_{mn}^{l(2)} &= T_{mn}^k C_{mn}^{l(1)}, \\ D_{mn}^{l(1)} &= R_{mn}^{k-1} C_{mn}^{l(1)}, & D_{mn}^{l(2)} &= R_{mn}^{k-1} T_{mn}^k C_{mn}^{l(1)}. \end{aligned}$$

Here, $\tilde{C}_{mn}^l, l = k-1, k-2, \dots, 0$, are calculated by the recursive formula (2.17) with $\tilde{C}_{mn}^k = 1$. Again, we can further rewrite the potential in a more concise form as

$$\Phi_l(\mathbf{r}, \mathbf{r}_s) = \frac{e_s}{\sqrt{\varepsilon_s \varepsilon_l(\tilde{\zeta})} a} \sum_{n=0}^{\infty} \sum_{m=0}^n \tilde{\mathcal{H}}_{mn} Y_n^m(\phi, \eta) \times \frac{F_{mn,lk}(\tilde{\zeta}, \tilde{\zeta}_s)}{1 - R_{mn}^{k-1} T_{mn}^k \gamma_{mn,k}}, \quad (2.27)$$

where

$$F_{mn,lk}(\tilde{\zeta}, \tilde{\zeta}_s) = \left[T_{mn}^k v_{mn}(\tilde{\zeta}_k) P_n^m(\tilde{\zeta}_s) + Q_n^m(\tilde{\zeta}_s) \right] \left[P_n^m(\tilde{\zeta}) + R_{mn}^{k-1} v_{mn}(\tilde{\zeta}_{l-1}) Q_n^m(\tilde{\zeta}) \right] \tilde{C}_{mn}^l,$$

with

$$\tilde{C}_{mn}^l = \prod_{j=1}^{k-1} \frac{T_{mn,j+1}}{1 - R_{mn,j+1} R_{mn}^{j-1} \gamma_{mn,j}}. \quad (2.28)$$

On the other hand, in the case of $k < l \leq L$, similar to Eq. (2.6b) we write the solution of Eq. (2.24) in the form

$$\Phi_l(\mathbf{r}, \mathbf{r}_s) = \frac{e_s}{\sqrt{\varepsilon_s \varepsilon_l(\tilde{\zeta})} a} \sum_{n=0}^{\infty} \sum_{m=0}^n \mathcal{H}_{mn}^P \left[v_{mn}(\tilde{\zeta}_l) C_{mn}^l P_n^m(\tilde{\zeta}) + D_{mn}^l Q_n^m(\tilde{\zeta}) \right] Y_n^m(\phi, \eta), \quad (2.29)$$

and accordingly rewrite $\Phi_k(\mathbf{r}, \mathbf{r}_s)$ as

$$\Phi_k(\mathbf{r}, \mathbf{r}_s) = \frac{e_s}{\sqrt{\varepsilon_s \varepsilon_k(\tilde{\zeta})} a} \sum_{n=0}^{\infty} \sum_{m=0}^n \mathcal{H}_{mn}^P \left[v_{mn}(\tilde{\zeta}_k) C_{mn}^k P_n^m(\tilde{\zeta}) + D_{mn}^k Q_n^m(\tilde{\zeta}) \right] Y_n^m(\phi, \eta),$$

where

$$C_{mn}^k = u_{mn}(\tilde{\zeta}_k) \times \frac{\bar{C}_{mn}^k}{\mathcal{H}_{mn}^P}, \quad D_{mn}^k = 1 + \frac{\bar{D}_{mn}^k}{\mathcal{H}_{mn}^P}.$$

Then, for $l = k+1, k+2, \dots, L$, we can calculate C_{mn}^l and D_{mn}^l in Eq. (2.29) using the recursive formula (2.11). Substituting them in Eq. (2.29) and rewriting the result, we get

$$\begin{aligned} \Phi_l(\mathbf{r}, \mathbf{r}_s) &= \frac{e_s}{\sqrt{\varepsilon_s \varepsilon_l(\tilde{\zeta})} a} \sum_{n=0}^{\infty} \sum_{m=0}^n \left[\left(\mathcal{H}_{mn}^Q \gamma_{mn,kl} C_{mn}^{l(1)} + \mathcal{H}_{mn}^P v_{mn}(\tilde{\zeta}_l) C_{mn}^{l(2)} \right) P_n^m(\tilde{\zeta}) \right. \\ &\quad \left. + \left(\mathcal{H}_{mn}^Q u_{mn}(\tilde{\zeta}_{k-1}) D_{mn}^{l(1)} + \mathcal{H}_{mn}^P D_{mn}^{l(2)} \right) Q_n^m(\tilde{\zeta}) \right] Y_n^m(\phi, \eta), \end{aligned} \quad (2.30)$$

where

$$\begin{aligned} D_{mn}^{l(2)} &= \frac{\tilde{D}_{mn}^l}{1 - R_{mn}^{k-1} T_{mn}^k \gamma_{mn,k}}, & D_{mn}^{l(1)} &= R_{mn}^{k-1} D_{mn}^{l(2)}, \\ C_{mn}^{l(2)} &= T_{mn}^k D_{mn}^{l(2)}, & C_{mn}^{l(1)} &= R_{mn}^{k-1} T_{mn}^k D_{mn}^{l(2)}. \end{aligned}$$

Here, \tilde{D}_{mn}^l , $l = k+1, k+2, \dots, L$, are calculated by the recursive formula (2.11) with $\tilde{D}_{mn}^k = 1$. Also, we can further rewrite the potential in the same concise form as (2.27) but with

$$F_{mn,lk}(\xi, \xi_s) = \left[T_{mn}^k v_{mn}(\xi_l) P_n^m(\xi) + Q_n^m(\xi) \right] \left[P_n^m(\xi_s) + R_{mn}^{k-1} u_{mn}(\xi_{k-1}) Q_n^m(\xi_s) \right] \tilde{D}_{mn}^l,$$

where

$$\tilde{D}_{mn}^l = \prod_{j=k+1}^l \frac{T_{mn,j}}{1 - R_{mn,j} T_{mn}^j \gamma_{mn,j}}. \quad (2.31)$$

Finally, it should be pointed out that the solution given by Eq. (2.6) for the case of $\xi_s \in [1, \xi_0]$ or Eq. (2.13) for the case of $\xi_s \in [\xi_{L-1}, \infty)$ can in fact be regarded as the special case of Eqs. (2.21) and (2.30) corresponding to $k=0$, or Eqs. (2.21) and (2.26) corresponding to $k=L$. Moreover, if we let

$$p_{mn,lk} = T_{mn}^k v_{mn}(\xi_l), \quad q_{mn,lk} = R_{mn}^{k-1} u_{mn}(\xi_{l-1}),$$

then in summary the generalized Coulomb potential at a point \mathbf{r} in the region l due to a point charge e_s at another point \mathbf{r}_s in the region k is given by

$$\Phi_{lk}(\mathbf{r}, \mathbf{r}_s) = \frac{e_s}{\sqrt{\varepsilon_l(\xi) \varepsilon_k(\xi_s) a}} \sum_{n=0}^{\infty} \sum_{m=0}^n \tilde{\mathcal{H}}_{mn} Y_n^m(\phi, \eta) \times \frac{F_{mn,lk}(\xi, \xi_s)}{(1 - p_{mn,kk} q_{mn,kk})}, \quad (2.32)$$

where the functions $F_{mn,lk}(\xi, \xi_s)$ are given by

$$F_{mn,lk}(\xi, \xi_s) = [p_{mn,kk} P_n^m(\xi_{>}) + Q_n^m(\xi_{>})] [P_n^m(\xi_{<}) + q_{mn,lk} Q_n^m(\xi_{<})] \tilde{C}_{mn}^l$$

if $l < k$,

$$F_{mn,lk}(\xi, \xi_s) = [p_{mn,kk} P_n^m(\xi_{>}) + Q_n^m(\xi_{>})] [P_n^m(\xi_{<}) + q_{mn,kk} Q_n^m(\xi_{<})]$$

for $l = k$, and

$$F_{mn,lk}(\xi, \xi_s) = [p_{mn,lk} P_n^m(\xi_{>}) + Q_n^m(\xi_{>})] [P_n^m(\xi_{<}) + q_{mn,kk} Q_n^m(\xi_{<})] \tilde{D}_{mn}^l$$

when $l > k$, and \tilde{C}_{mn}^l and \tilde{D}_{mn}^l are given in (2.28) and (2.31), respectively.

2.5 Formula for the self-polarization energy

From Eq. (2.21) or (2.32), the self-polarization energy at a point \mathbf{r} in the region k where $0 \leq k \leq L$, denoted by $V_s^k(\mathbf{r})$, can be calculated by taking $\mathbf{r} = \mathbf{r}_s, e = e_s$, excluding the direct Coulomb interaction from $\Phi_k(\mathbf{r}, \mathbf{r}_s)$, and dividing by 2 as it corresponds to a self-energy, namely,

$$V_s^k(\mathbf{r}) = \frac{1}{2} e \Phi_k(\mathbf{r}, \mathbf{r}).$$

Thus we have

$$V_s^k(\mathbf{r}) = \frac{e^2}{2\varepsilon_k(\xi)a} \sum_{n=0}^{\infty} \sum_{m=0}^n \mathcal{H}_{mn} \left(\gamma_{mn,k} C_{mn}^{k(1)} P_n^m(\xi) Q_n^m(\xi) + v_{mn}(\xi_k) C_{mn}^{k(2)} P_n^{m2}(\xi) + u_{mn}(\xi_{k-1}) D_{mn}^{k(1)} Q_n^{m2}(\xi) + \gamma_{mn,k} D_{mn}^{k(2)} P_n^m(\xi) Q_n^m(\xi) \right) P_n^{m2}(\eta),$$

where the coefficients $C_{mn}^{k(1)}, C_{mn}^{k(2)}, D_{mn}^{k(1)}$, and $D_{mn}^{k(2)}$ are given by Eq. (2.22), or

$$V_s^k(\mathbf{r}) = \frac{e^2}{2\varepsilon_k(\xi)a} \sum_{n=0}^{\infty} \sum_{m=0}^n \frac{\mathcal{H}_{mn} P_n^{m2}(\eta)}{(1 - p_{mn,kk} q_{mn,kk})} \times \left[p_{mn,kk} P_n^{m2}(\xi) + p_{mn,kk} q_{mn,kk} P_n^m(\xi) Q_n^m(\xi) + q_{mn,kk} Q_n^{m2}(\xi) \right].$$

3 Extension to the oblate spheroidal geometry

The results obtained for the prolate spheroidal geometry can be readily extended to the oblate spheroidal geometry if the corresponding oblate spheroidal coordinates (ξ, η, ϕ) are defined through

$$x = \frac{a}{2} \sqrt{(1 + \xi^2)(1 - \eta^2)} \cos \phi, \quad y = \frac{a}{2} \sqrt{(1 + \xi^2)(1 - \eta^2)} \sin \phi, \quad z = \frac{a}{2} \xi \eta,$$

where a is the interfocal distance of the oblate spheroid, $\xi \in [0, \infty)$ is the radial variable, $\eta \in [-1, 1]$ is the angular variable, and $\phi \in [0, 2\pi]$ is the azimuthal variable, respectively. Under this definition, the surface of constant ξ is an oblate spheroid with the interfocal distance a . In particular, the surface of $\xi = 0$ is the circular disk in the plane $z = 0$ with radius $a/2$. Then all the results obtained for prolate spheroids can be extended to oblate spheroids basically by following this rule: replace ξ by $i\xi$ where $i = \sqrt{-1}$ and \mathcal{H}_{mn} by

$$\hat{\mathcal{H}}_{mn} = 2i(2n + 1)(2 - \delta_{m0})(-1)^m \left[\frac{(n - m)!}{(n + m)!} \right]^2.$$

For example, a quasi-harmonic three-layer dielectric permittivity profile can be given by

$$\hat{\varepsilon}(\xi) = \varepsilon(i\xi) = \begin{cases} \varepsilon_i, & \text{if } \xi \leq \xi_I, \\ \left[\alpha + \frac{\beta}{2} \ln \left(\frac{i\xi + 1}{i\xi - 1} \right) \right]^2, & \text{if } \xi_I < \xi < \xi_O, \\ \varepsilon_o, & \text{if } \xi \geq \xi_O, \end{cases} \quad (3.1)$$

where

$$\alpha = \frac{c\sqrt{\varepsilon_o} - d\sqrt{\varepsilon_i}}{c-d}, \quad \beta = \frac{\sqrt{\varepsilon_i} - \sqrt{\varepsilon_o}}{c-d},$$

with

$$c = \frac{1}{2} \ln \left(\frac{i\zeta_I + 1}{i\zeta_I - 1} \right), \quad d = \frac{1}{2} \ln \left(\frac{i\zeta_O + 1}{i\zeta_O - 1} \right).$$

Note that now β is a pure imaginary number. Actually, using the fact that

$$Q_0^0(i\zeta) \equiv \frac{1}{2} \ln \left(\frac{i\zeta + 1}{i\zeta - 1} \right) = i \left(\tan^{-1}(\zeta) - \frac{\pi}{2} \right),$$

the quasi-harmonic three-layer dielectric model given by (3.1) can be rewritten as

$$\hat{\varepsilon}(\zeta) = \begin{cases} \varepsilon_i, & \text{if } \zeta \leq \zeta_I, \\ \left(\hat{\alpha} - \hat{\beta} \tan^{-1} \zeta \right)^2, & \text{if } \zeta_I < \zeta < \zeta_O, \\ \varepsilon_o, & \text{if } \zeta \geq \zeta_O, \end{cases} \quad (3.2)$$

where

$$\hat{\alpha} = \frac{\hat{c}\sqrt{\varepsilon_o} - \hat{d}\sqrt{\varepsilon_i}}{\hat{c} - \hat{d}}, \quad \hat{\beta} = \frac{\sqrt{\varepsilon_o} - \sqrt{\varepsilon_i}}{\hat{c} - \hat{d}},$$

with

$$\hat{c} = \tan^{-1}(\zeta_I), \quad \hat{d} = \tan^{-1}(\zeta_O).$$

In this form, $\hat{\beta}$ is a real number, and in fact $\hat{\beta} = -\beta i$ or $\beta = \hat{\beta} i$.

4 Numerical experiments

In this section, we apply the proposed numerical method to the calculation of the self-polarization energy of a prolate spheroidal quantum dot (QD). In particular, we consider the QD given by $(x^2 + y^2)/a_1^2 + z^2/a_2^2 = 1$ with $a_1 = 10 \text{ \AA}$, $a_2 = 20 \text{ \AA}$, $\varepsilon_i = 12.6$ (GaAs), and $\varepsilon_o = 1$ (vacuum), which leads to $\zeta_b \approx 1.1547$. In all simulations, the imposed upper limit of n is set to $N = 40$. Unless otherwise specified, all analytical results and illustrative plots are based on the calculation of the self-polarization energies of 1000 unit charges (in atomic unit) uniformly distributed along the ray pointing to the point $(10, 0, 20)$. Furthermore, the number of steps used to discretize the translation layer is set to $L = 1000$.

4.1 The quasi-harmonic dielectric model as $\delta \rightarrow 0$

Fig. 5 plots the self-polarization energy V_s for the QD corresponding to the quasi-harmonic model and the analytical solution (see Appendix B) with several different δ values, along a minor axis of the prolate spheroidal QD and along the ray pointing to the point $(10, 0, 20)$, respectively. It is well-known that under the step-like model, when

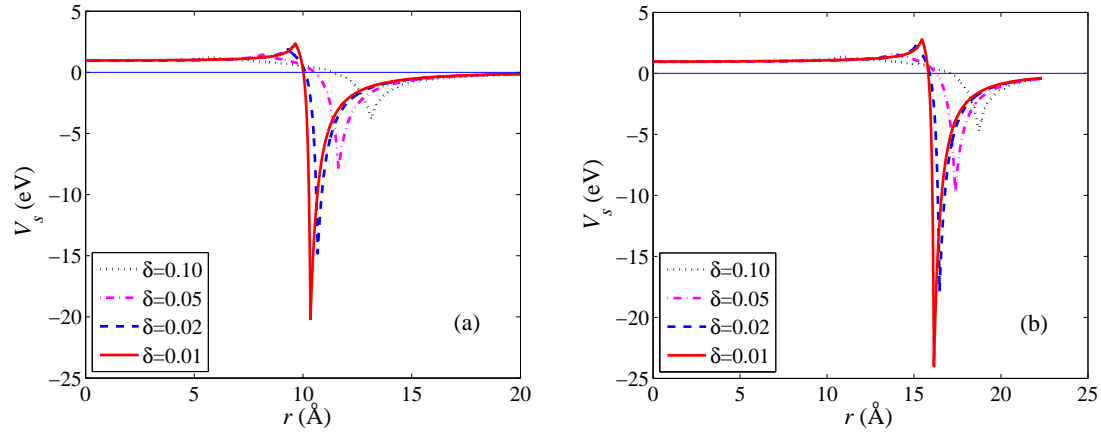


Figure 5: Self-polarization energy V_s of a prolate spheroidal QD as a function of r corresponding to the quasi-harmonic model with $\delta=0.01,0.02,0.05$ and 0.1 . (a) along a minor axis of the prolate spheroidal QD, and (b) along the ray pointing to the point $(10,0,20)$.

the source charge is placed in the region with a higher dielectric constant, the induced charges have the same sign as the source charge and the interaction between the source and the induced charges is repulsive. On the contrary, if the source charge is located in the region with a lower dielectric constant, the induced charges have an opposite sign as the source charge and the interaction is attractive. As can be seen from Fig. 5, under the quasi-harmonic model, the self-polarization energy remains positive inside the dot ($r \leq 10$ Å for Fig. 5 (a) or $r \leq 15.8114$ Å for Fig. 5 (b)), and the positive potential extends to the outside of the dot to some extent. As the translation layer decreases in size, however, the self-polarization energy given by the analytical solution for the quasi-harmonic model will reduce to that for the step-like model (not shown in the graphs). In addition, it can be observed that, the quasi-harmonic model leads to differential singularity in the self-polarization potential energy at the both edges of the translation layer, precisely where the derivative of $\varepsilon(\xi)$ is discontinuous.

4.2 Validation of the proposed numerical method and its implementation

Fig. 6 plots the self-polarization energy for the QD corresponding to the quasi-harmonic dielectric model with $\delta = 0.1$ by using the analytical solution and the proposed numerical method using several different L values. For the quasi-harmonic dielectric model, its L -step approximation described in Section 2.1 is actually exact, suggesting that, for the quasi-harmonic dielectric model, the proposed numerical method with any $L (\geq 2)$ value should give us the exact solution of the Poisson equation. As shown in Fig. 6, the numerical solutions with different L values and the analytical solution which was obtained in a different manner are indeed indistinguishable, thus validating the correctness of the proposed numerical method and its implementation.

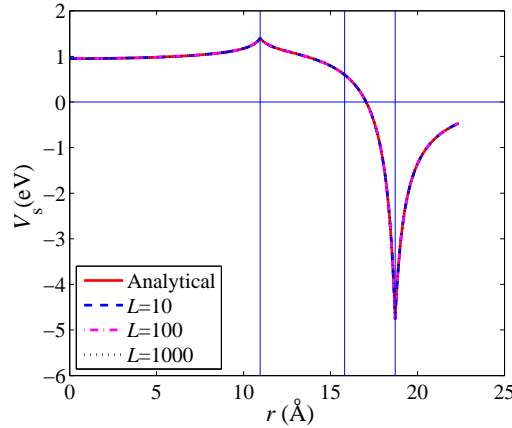


Figure 6: Self-polarization energy V_s as a function of r corresponding to the quasi-harmonic dielectric model with $\delta=0.1$. Solid line, the analytical solution; dashed line, the numerical solution with $L=10$; dot-dashed line, the numerical solution with $L=100$; and dotted line, the numerical solution with $L=1000$.

4.3 Convergence of the proposed numerical method as $L \rightarrow \infty$

To investigate the convergence of the proposed numerical method in terms of L , here we consider its application to the linear and the cosine-like dielectric models with $\delta=0.1$. We calculate the self-polarization energies of 1000 unit charges equally spaced along the ray pointing to the point $(10,0,20)$, and the numerical results are compared to those obtained by the proposed numerical method using $L=10,000$ to calculate the L_2 -relative errors in the self-polarization energy, which are displayed in Fig. 7. As can be seen, the results clearly demonstrate the convergence of the proposed numerical method as $L \rightarrow \infty$. Based on this, it is reasonable to believe that, for general three-layer dielectric models, the proposed numerical method should be able to recover the exact solution of the corresponding Poisson equation as $L \rightarrow \infty$. The results also seem to indicate that, using the same L value, the error corresponding to the linear model is smaller, which can be understood in part by the fact that the L -step approximation of the linear model described in Section 2.1 seems to be more accurate than that of the cosine-like model, as indicated by Fig. 4.

4.4 Comparison among the three three-layer dielectric models

In Fig. 8 we show the self-polarization energy for the QD corresponding to the foregoing three three-layer dielectric models with $\delta=0.02$ and $\delta=0.1$, respectively. It is clear that the choice of different dielectric permittivity profiles for the dielectric translation layer modifies both the strength and the functional form of the potentials, although all three forms of $\varepsilon(\tilde{\zeta})$ can eliminate the mathematical divergence present when $\delta=0$. However, since the derivative of $\varepsilon(\tilde{\zeta})$ in both the quasi-harmonic and the linear models is discontinuous at the both edges of the translation layer, the self-polarization energy corresponding to

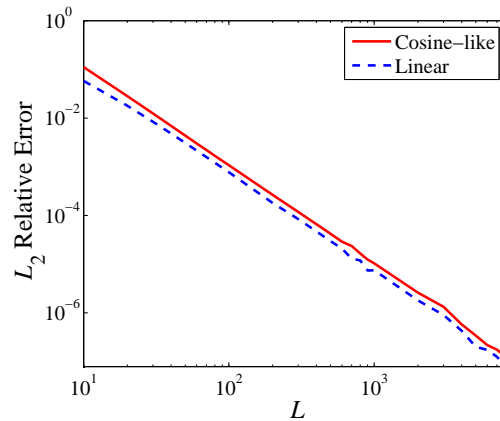


Figure 7: L_2 -relative error in the self-polarization energy corresponding to the linear and the cosine-like models with $\delta=0.1$, respectively, using the proposed numerical method with various L values.

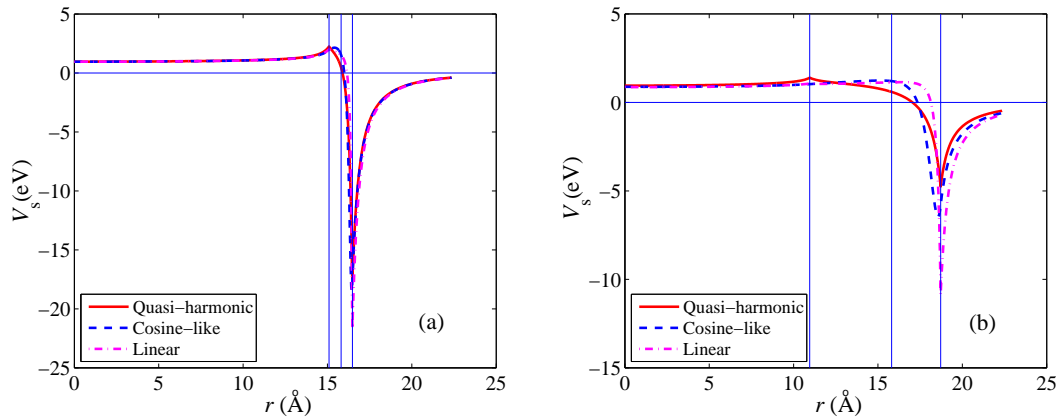


Figure 8: Self-polarization energy V_s as a function of r for several three-layer dielectric models with (a) $\delta=0.02$ and (b) $\delta=0.1$, respectively. Solid line, the quasi-harmonic model with using the analytical solution; dashed and dot-dashed lines, the cosine-like and the linear models with using the proposed numerical method.

these two models exhibits differential singularity at these locations as well. Fortunately, this singularity is integrable. Also as it shows, in general as the translation layer decreases in size, like for the quasi-harmonic dielectric model, the self-polarization energy for the linear or cosine-like dielectric model obtained by the proposed numerical method again appears to reduce to that for the step-like model (not shown in the graphs).

5 Conclusions

In this paper, based on the novel quasi-harmonic three-layer dielectric model for the interface between a dielectric spheroid and the surrounding dissimilar dielectric medium,

we have presented a robust numerical method for calculating the generalized Coulomb and self-polarization potential energies of such a dielectric spheroid. The proposed numerical method can not only overcome the inherent mathematical divergence in the self-polarization energy which arises for the simplest step-like model of the dielectric interface, but also completely eliminate the potential numerical divergence which may occur in other treatments. Numerical experiments have demonstrated the convergence of the proposed numerical method as the number of the steps used to discretize the translation layer in a general three-layer model goes to infinity. The proposed numerical method may find its application in many areas that involve the calculation of the generalized Coulomb potential, including the calculation of self-polarization energies of quantum dots with finite confinement barriers and the calculation of electrostatic interactions in the hybrid explicit/implicit solvation models in biomolecular simulations. Presently, we are in the process of applying this numerical method to the investigation of the energy spectrum and other characteristics of a spheroidal quantum dot with an off-centered shallow donor impurity located anywhere inside the dot, and any significant findings will be reported in future publications.

Acknowledgments

C. Xue would like to thank the support of the National Natural Science Foundation of China (Grant No. 10971181), and S. Deng would like to thank the support of the National Institutes of Health (Grant No. 1R01GM083600-03), for the work reported in this paper.

A Analytical solution for the step-like dielectric model

The Poisson equation (1.1) can be solved analytically if we assume that the radial ζ -dependence for $\varepsilon(\mathbf{r})$ corresponds to the step-like model, as shown in Fig. 9. The dielectric constants for the prolate spheroid and the surrounding medium are ε_i and ε_o , respectively. The point charge e_s is assumed to be located, without loss of generality, at the point $\mathbf{r}_s = (\zeta_s, \eta_s, \phi_s = 0)$ in the xz -plane inside or outside the dielectric spheroid defined by the equation $\zeta = \zeta_b$. The interfocal distance of the prolate spheroid is a .

The analytical solution to this electrostatic problem is given in [36, 37]. In short, the potential Φ_o or Φ_i at an observation point $\mathbf{r} = (\zeta, \eta, \phi)$ outside or inside the spheroid, respectively, due to a point charge e_s inside the prolate spheroid (so $\zeta_b > \zeta_s \geq 1$) is given by

$$\Phi_o(\mathbf{r}, \mathbf{r}_s) = \frac{e_s}{\varepsilon_i a} \sum_{n=0}^{\infty} \sum_{m=0}^n \varepsilon_i \mathcal{H}_{mn}^P \Delta_{mn} K_{mn}^{-1} Q_n^m(\zeta) Y_n^m(\phi, \eta), \quad (\text{A.1a})$$

$$\Phi_i(\mathbf{r}, \mathbf{r}_s) = \frac{e_s}{\varepsilon_i |\mathbf{r} - \mathbf{r}_s|} + \frac{e_s}{\varepsilon_i a} \sum_{n=0}^{\infty} \sum_{m=0}^n (\varepsilon_i - \varepsilon_o) \mathcal{H}_{mn}^P Q_n^m(\zeta_b) \hat{Q}_n^m(\zeta_b) K_{mn}^{-1} P_n^m(\zeta) Y_n^m(\phi, \eta), \quad (\text{A.1b})$$

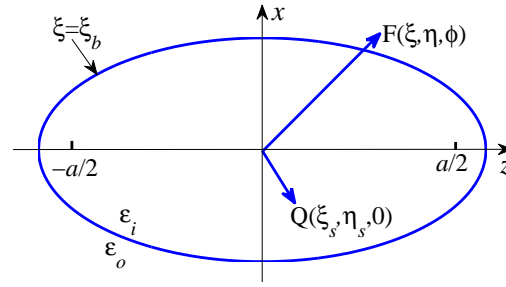


Figure 9: Schematic illustration of the step-like dielectric model: the dielectric constants of a prolate spheroid and the surrounding medium are ϵ_i and ϵ_o , respectively. The prolate spheroid, defined by the equation $\xi = \xi_b$, has an interfocal distance a . A point charge e_s is located at the point $\mathbf{r}_s = (\xi_s, \eta_s, \phi_s = 0)$ in the xz -plane.

where

$$\begin{aligned} \Delta_{mn} &= P_n^m(\xi_b) \hat{Q}_n^m(\xi_b) - Q_n^m(\xi_b) \hat{P}_n^m(\xi_b), \\ K_{mn} &= \epsilon_o P_n^m(\xi_b) \hat{Q}_n^m(\xi_b) - \epsilon_i Q_n^m(\xi_b) \hat{P}_n^m(\xi_b), \\ \hat{P}_n^m(\xi) &= (n - m + 1) P_{n+1}^m(\xi) - (n + 1) \xi P_n^m(\xi), \\ \hat{Q}_n^m(\xi) &= (n - m + 1) Q_{n+1}^m(\xi) - (n + 1) \xi Q_n^m(\xi). \end{aligned}$$

On the other hand, if the charge e_s is located at the point $\mathbf{r}_s = (\xi_s, \eta_s, \phi_s = 0)$ outside the prolate spheroid (so $\xi_s > \xi_b > 1$), we have

$$\Phi_o(\mathbf{r}, \mathbf{r}_s) = \frac{e_s}{\epsilon_o |\mathbf{r} - \mathbf{r}_s|} + \frac{e_s}{\epsilon_o a} \sum_{n=0}^{\infty} \sum_{m=0}^n (\epsilon_i - \epsilon_o) \mathcal{H}_{mn}^Q P_n^m(\xi_b) \hat{P}_n^m(\xi_b) K_{mn}^{-1} Q_n^m(\xi) Y_n^m(\phi, \eta), \quad (\text{A.2a})$$

$$\Phi_i(\mathbf{r}, \mathbf{r}_s) = \frac{e_s}{\epsilon_o a} \sum_{n=0}^{\infty} \sum_{m=0}^n \epsilon_o \mathcal{H}_{mn}^Q \Delta_{mn} K_{mn}^{-1} P_n^m(\xi) Y_n^m(\phi, \eta). \quad (\text{A.2b})$$

Accordingly, the self-polarization energy is given as follows.

$$V_s(\mathbf{r}) = \begin{cases} \frac{e^2}{2\epsilon_o a} \sum_{n=0}^{\infty} \sum_{m=0}^n (\epsilon_i - \epsilon_o) \mathcal{H}_{mn} P_n^m(\xi_b) \hat{P}_n^m(\xi_b) K_{mn}^{-1} Q_n^{m2}(\xi) P_n^{m2}(\eta), & \text{if } \xi \geq \xi_b, \\ \frac{e^2}{2\epsilon_i a} \sum_{n=0}^{\infty} \sum_{m=0}^n (\epsilon_i - \epsilon_o) \mathcal{H}_{mn} Q_n^m(\xi_b) \hat{Q}_n^m(\xi_b) K_{mn}^{-1} P_n^{m2}(\xi) P_n^{m2}(\eta), & \text{if } \xi < \xi_b. \end{cases} \quad (\text{A.3})$$

B Analytical solution for the quasi-harmonic dielectric model

The analytical solution to the Poisson equation (1.1) corresponding to the proposed quasi-harmonic dielectric model (2.3) is easy to find [43]. The key in obtaining the analytical solution for the quasi-harmonic model is this important observation [9]: If $\epsilon(\mathbf{r})$ in the quasi-harmonic equation $\nabla \cdot (\epsilon(\mathbf{r}) \nabla \phi(\mathbf{r})) = 0$ satisfies $\Delta \sqrt{\epsilon(\mathbf{r})} = 0$, then $\Delta(\sqrt{\epsilon(\mathbf{r})} \phi(\mathbf{r})) = 0$.

Similarly, if $\varepsilon(\mathbf{r})$ in the quasi-elliptic equation $\nabla \cdot (\varepsilon(\mathbf{r}) \nabla \phi(\mathbf{r})) = \rho(\mathbf{r})$ satisfies $\Delta \sqrt{\varepsilon(\mathbf{r})} = 0$, then

$$\Delta \left(\sqrt{\varepsilon(\mathbf{r})} \phi(\mathbf{r}) \right) = \frac{\rho(\mathbf{r})}{\sqrt{\varepsilon(\mathbf{r})}}.$$

Since by construction, $\Delta \sqrt{\varepsilon(\xi)} = 0$ in the translation layer, the electrostatic potential in this layer, Φ_t , can thus be expressed as

$$\Phi_t(\mathbf{r}, \mathbf{r}_s) = \frac{e_s}{\sqrt{\varepsilon(\xi)}} \sum_{n=0}^{\infty} \sum_{m=0}^n (C_{mn} P_n^m(\xi) + D_{mn} Q_n^m(\xi)) Y_n^m(\phi, \eta),$$

or, when the charge e_s itself is also located inside the translation layer, as

$$\Phi_t(\mathbf{r}, \mathbf{r}_s) = \frac{e_s}{\sqrt{\varepsilon_s \varepsilon(\xi)} |\mathbf{r} - \mathbf{r}_s|} + \frac{e_s}{\sqrt{\varepsilon(\xi)}} \sum_{n=0}^{\infty} \sum_{m=0}^n (C_{mn} P_n^m(\xi) + D_{mn} Q_n^m(\xi)) Y_n^m(\phi, \eta),$$

where $\varepsilon_s = \varepsilon(\xi_s)$, C_{mn} and D_{mn} are constant expansion coefficients.

Again without loss of generality, a point charge e_s is assumed to be located at the point $\mathbf{r}_s = (\xi_s, \eta_s, \phi_s = 0)$ in the xz -plane. Then, when e_s is located inside the inner layer ($1 \leq \xi_s \leq \xi_I = \xi_b - \delta$), the potential in the outer layer Φ_o , the potential in the inner layer Φ_i , and the potential in the translation layer Φ_t are written as

$$\Phi_o(\mathbf{r}, \mathbf{r}_s) = \frac{e_s}{\sqrt{\varepsilon_i \varepsilon_o} a} \sum_{n=0}^{\infty} \sum_{m=0}^n \mathcal{H}_{mn}^P A_{mn}^{(1)} Q_n^m(\xi) Y_n^m(\phi, \eta), \quad (\text{B.1a})$$

$$\Phi_i(\mathbf{r}, \mathbf{r}_s) = \frac{e_s}{\varepsilon_i |\mathbf{r} - \mathbf{r}_s|} + \frac{e_s}{\varepsilon_i a} \sum_{n=0}^{\infty} \sum_{m=0}^n \mathcal{H}_{mn}^P v_{mn}(\xi_I) B_{mn}^{(1)} P_n^m(\xi) Y_n^m(\phi, \eta), \quad (\text{B.1b})$$

$$\Phi_t(\mathbf{r}, \mathbf{r}_s) = \frac{e_s}{\sqrt{\varepsilon_i \varepsilon(\xi)} a} \sum_{n=0}^{\infty} \sum_{m=0}^n \mathcal{H}_{mn}^P \left(v_{mn}(\xi_O) C_{mn}^{(1)} P_n^m(\xi) + D_{mn}^{(1)} Q_n^m(\xi) \right) Y_n^m(\phi, \eta), \quad (\text{B.1c})$$

where the constant expansion coefficients $A_{mn}^{(1)}$, $B_{mn}^{(1)}$, $C_{mn}^{(1)}$, and $D_{mn}^{(1)}$ are determined by the boundary condition at the two edges of the translation layer, together with the orthogonality of $\cos(m\phi)$ and that of the associated Legendre polynomials $P_n^m(\dots)$, and the expansion of the reciprocal distance in the prolate spheroidal coordinates (2.7). Omitting all details, for $n=0, 1, \dots$, and $m=0, 1, \dots, n$, we have

$$\mathbf{M}^{(1)} \times \begin{pmatrix} A_{mn}^{(1)} \\ B_{mn}^{(1)} \\ C_{mn}^{(1)} \\ D_{mn}^{(1)} \end{pmatrix} = \begin{pmatrix} -1 \\ 0 \\ -\bar{Q}_n^m(\xi_I) \\ 0 \end{pmatrix},$$

with

$$\mathbf{M}^{(1)} = \begin{bmatrix} 0, & 1, & -\gamma_{mn}, & -1 \\ 1, & 0, & -1, & -1 \\ 0, & \bar{P}_n^m(\xi_I), & \left(-\bar{P}_n^m(\xi_I) - \frac{\beta}{\sqrt{\varepsilon_i}}\right)\gamma_{mn}, & -\bar{Q}_n^m(\xi_I) - \frac{\beta}{\sqrt{\varepsilon_i}} \\ \bar{Q}_n^m(\xi_O), & 0, & -\bar{P}_n^m(\xi_O) - \frac{\beta}{\sqrt{\varepsilon_o}}, & -\bar{Q}_n^m(\xi_O) - \frac{\beta}{\sqrt{\varepsilon_o}} \end{bmatrix},$$

where $\gamma_{mn} = u_{mn}(\xi_I)v_{mn}(\xi_O)$.

Similarly, if e_s is located inside the outer layer ($\xi_s \geq \xi_O = \xi_b + \delta$), we can write

$$\Phi_o(\mathbf{r}, \mathbf{r}_s) = \frac{e_s}{\varepsilon_o |\mathbf{r} - \mathbf{r}_s|} + \frac{e_s}{\varepsilon_o a} \sum_{n=0}^{\infty} \sum_{m=0}^n \mathcal{H}_{mn}^Q u_{mn}(\xi_O) A_{mn}^{(2)} Q_n^m(\xi) Y_n^m(\phi, \eta), \tag{B.2a}$$

$$\Phi_i(\mathbf{r}, \mathbf{r}_s) = \frac{e_s}{\sqrt{\varepsilon_o \varepsilon_i} a} \sum_{n=0}^{\infty} \sum_{m=0}^n \mathcal{H}_{mn}^Q B_{mn}^{(2)} P_n^m(\xi) Y_n^m(\phi, \eta), \tag{B.2b}$$

$$\Phi_t(\mathbf{r}, \mathbf{r}_s) = \frac{e_s}{\sqrt{\varepsilon_o \varepsilon(\xi)} a} \sum_{n=0}^{\infty} \sum_{m=0}^n \mathcal{H}_{mn}^Q \left(C_{mn}^{(2)} P_n^m(\xi) + u_{mn}(\xi_I) D_{mn}^{(2)} Q_n^m(\xi) \right) Y_n^m(\phi, \eta), \tag{B.2c}$$

where the expansion coefficients $A_{mn}^{(2)}, B_{mn}^{(2)}, C_{mn}^{(2)}$, and $D_{mn}^{(2)}$ are determined by

$$\mathbf{M}^{(2)} \times \begin{pmatrix} A_{mn}^{(2)} \\ B_{mn}^{(2)} \\ C_{mn}^{(2)} \\ D_{mn}^{(2)} \end{pmatrix} = \begin{pmatrix} 0 \\ -1 \\ 0 \\ -\bar{P}_n^m(\xi_O) \end{pmatrix},$$

with

$$\mathbf{M}^{(2)} = \begin{bmatrix} 0, & 1, & -1, & -1 \\ 1, & 0, & -1, & -\gamma_{mn} \\ 0, & \bar{P}_n^m(\xi_I), & -\bar{P}_n^m(\xi_I) - \frac{\beta}{\sqrt{\varepsilon_i}}, & -\bar{Q}_n^m(\xi_I) - \frac{\beta}{\sqrt{\varepsilon_i}} \\ \bar{Q}_n^m(\xi_O), & 0, & -\bar{P}_n^m(\xi_O) - \frac{\beta}{\sqrt{\varepsilon_o}}, & \left(-\bar{Q}_n^m(\xi_O) - \frac{\beta}{\sqrt{\varepsilon_o}}\right)\gamma_{mn} \end{bmatrix}.$$

Finally, when e_s is located inside the translation layer ($\xi_I < \xi_s < \xi_O$), we can write

$$\Phi_o(\mathbf{r}, \mathbf{r}_s) = \frac{e_s}{\sqrt{\varepsilon_s \varepsilon_o} a} \sum_{n=0}^{\infty} \sum_{m=0}^n \left[\mathcal{H}_{mn}^Q u_{mn}(\xi_I) A_{mn}^{(3)} + \mathcal{H}_{mn}^P v_{mn}(\xi_O) A_{mn}^{(4)} \right] Q_n^m(\xi) Y_n^m(\phi, \eta), \tag{B.3a}$$

$$\Phi_i(\mathbf{r}, \mathbf{r}_s) = \frac{e_s}{\sqrt{\varepsilon_s \varepsilon_i} a} \sum_{n=0}^{\infty} \sum_{m=0}^n \left[\mathcal{H}_{mn}^Q B_{mn}^{(3)} + \mathcal{H}_{mn}^P v_{mn}(\xi_O) B_{mn}^{(4)} \right] P_n^m(\xi) Y_n^m(\phi, \eta), \tag{B.3b}$$

$$\begin{aligned} \Phi_I(\mathbf{r}, \mathbf{r}_s) &= \frac{e_s}{\sqrt{\varepsilon_s \varepsilon(\xi)} |\mathbf{r} - \mathbf{r}_s|} + \frac{e_s}{\sqrt{\varepsilon_s \varepsilon(\xi)} a} \\ &\times \sum_{n=0}^{\infty} \sum_{m=0}^n \left[\left(\mathcal{H}_{mn}^Q \gamma_{mn} C_{mn}^{(3)} + \mathcal{H}_{mn}^P v_{mn}(\xi_O) C_{mn}^{(4)} \right) P_n^m(\xi) \right. \\ &\quad \left. + \left(\mathcal{H}_{mn}^Q u_{mn}(\xi_I) D_{mn}^{(3)} + \mathcal{H}_{mn}^P \gamma_{mn} D_{mn}^{(4)} \right) Q_n^m(\xi) \right] Y_n^m(\phi, \eta), \end{aligned} \quad (\text{B.3c})$$

where, the expansion coefficients $A_{mn}^{(3)}, B_{mn}^{(3)}, C_{mn}^{(3)}$, and $D_{mn}^{(3)}$ are determined by

$$\mathbf{M}^{(1)} \times \begin{pmatrix} A_{mn}^{(3)} \\ B_{mn}^{(3)} \\ C_{mn}^{(3)} \\ D_{mn}^{(3)} \end{pmatrix} = \begin{pmatrix} 1 \\ 0 \\ \bar{P}_n^m(\xi_I) + \frac{\beta}{\sqrt{\varepsilon_i}} \\ 0 \end{pmatrix},$$

and the expansion coefficients $A_{mn}^{(4)}, B_{mn}^{(4)}, C_{mn}^{(4)}$, and $D_{mn}^{(4)}$ are determined by

$$\mathbf{M}^{(2)} \times \begin{pmatrix} A_{mn}^{(4)} \\ B_{mn}^{(4)} \\ C_{mn}^{(4)} \\ D_{mn}^{(4)} \end{pmatrix} = \begin{pmatrix} 0 \\ 1 \\ 0 \\ \bar{Q}_n^m(\xi_O) + \frac{\beta}{\sqrt{\varepsilon_o}} \end{pmatrix}.$$

From Eqs. (B.1)-(B.3), one can arrive at the self-polarization potential energy of a charged particle e at the location \mathbf{r} as follows.

$$V_s(\mathbf{r}) = \begin{cases} \frac{e^2}{2\varepsilon_o a} \sum_{n=0}^{\infty} \sum_{m=0}^n \mathcal{H}_{mn} u_{mn}(\xi_O) A_{mn}^{(2)} Q_n^{m2}(\xi) P_n^{m2}(\eta), & \text{if } \xi \geq \xi_O, \\ \frac{e^2}{2\varepsilon_i a} \sum_{n=0}^{\infty} \sum_{m=0}^n \mathcal{H}_{mn} v_{mn}(\xi_I) B_{mn}^{(1)} P_n^{m2}(\xi) P_n^{m2}(\eta), & \text{if } \xi \leq \xi_I, \\ \frac{e^2}{2\varepsilon(\xi) a} \sum_{n=0}^{\infty} \sum_{m=0}^n \mathcal{H}_{mn} \left(\gamma_{mn} C_{mn}^{(3)} P_n^m(\xi) Q_n^m(\xi) + v_{mn}(\xi_O) C_{mn}^{(4)} P_n^{m2}(\xi) \right. \\ \quad \left. + u_{mn}(\xi_I) D_{mn}^{(3)} Q_n^{m2}(\xi) + \gamma_{mn} D_{mn}^{(4)} P_n^m(\xi) Q_n^m(\xi) \right) P_n^{m2}(\eta), & \text{if } \xi_I < \xi < \xi_O. \end{cases}$$

References

- [1] L. E. Brus, Electron-electron and electron-hole interactions in small semiconductor crystallites: The size dependence of the lowest excited electronic state, J. Chem. Phys. 80 (1984) 4403.
- [2] M. Lannoo, C. Delerue, G. Allan, Screening in semiconductor nanocrystallites and its consequences for porous silicon, Phys. Rev. Lett. 74 (1995) 3415–3418.

- [3] P. G. Bolcatto, C. R. Proetto, Partially confined excitons in semiconductor nanocrystals with a finite size dielectric interface, *J. Phys. Condens. Matter* 13 (2001) 319–334.
- [4] A. Okur, C. Simmerling, Hybrid explicit/implicit solvation methods, in: D. C. Spellmeyer (Ed.), *Annu. Rep. Comput. Chem.*, Vol. 2, Chemistry of the American Chemical Society, 2006, Ch. 6, pp. 97–109.
- [5] D. B. Tran Thoai, R. Zimmermann, M. Grundmann, D. Bimberg, Image charges in semiconductor quantum wells: Effect on exciton binding energy, *Phys. Rev. B* 42 (1990) 5906–5909.
- [6] L. Bányai, P. Gilliot, Y. Z. Hu, S. W. Koch, Surface-polarization instabilities of electron-hole pairs in semiconductor quantum dots, *Phys. Rev. B* 45 (1992) 14136–14142.
- [7] P. G. Bolcatto, C. R. Proetto, Self-polarization energies of semiconductor quantum dots with finite confinement barriers, *Phys. Stat. Sol.* 220 (2000) 191–194.
- [8] J. L. Movilla, J. Planelles, Image charges in spherical quantum dots with an off-centered impurity: algorithm and numerical results, *Comput. Phys. Commun.* 170 (2005) 144–152.
- [9] P. Qin, Z. Xu, W. Cai, D. Jacobs, Image charge methods for a three-dielectric-layer hybrid solvation model of biomolecules, *Commun. Comput. Phys.* 6 (2009) 955–977.
- [10] S. Deng, A robust numerical method for self-polarization energy of spherical quantum dots with finite confinement barriers, *Comput. Phys. Commun.* 181 (2010) 787–799.
- [11] M. Feig, C. L. Brooks III, Recent advances in the development and application of implicit solvent models in biomolecule simulations, *Curr. Opin. Struct. Biol.* 14 (2004) 217–224.
- [12] N. A. Baker, Improving implicit solvent simulations: a Poisson-centric view, *Curr. Opin. Struct. Biol.* 15 (2005) 137–143.
- [13] T. Lazaridis, M. Karplus, Effective energy function for proteins in solution, *Proteins: Struct., Funct., Genet.* 35 (1999) 133–152.
- [14] A. Warshel, M. Levitt, Theoretical studies of enzymic reactions: Dielectric, electrostatic and steric stabilization of the carbonium ion in the reaction of lysozyme, *J. Mol. Biol.* 103 (1976) 227–249.
- [15] A. Warshel, Conversion of light energy to electrostatic energy in the proton pump of *Halobacterium halobium*, *Photochem. Photobiol.* 30 (1979) 285–290.
- [16] B. E. Hingerty, R. H. Ritchie, T. L. Ferrell, J. E. Turner, Dielectric effects in biopolymers: The theory of ionic saturation revisited, *Biopolymers* 24 (1985) 427–439.
- [17] J. Ramstein, R. Lavery, Energetic coupling between DNA bending and base pair opening, *Proc. Natl. Acad. Sci. USA.* 85 (1988) 7231–7235.
- [18] M. Shen, K. F. Freed, All-atom fast protein folding simulations: The villin headpiece, *Proteins: Struct. Funct. Genet.* 49 (2002) 439–445.
- [19] A. K. Jha, K. F. Freed, Solvation effect on conformations of 1,2-Dimethoxyethane: Charge dependent nonlinear response in implicit solvent models, *J. Chem. Phys.* 128 (2008) 034501.
- [20] B. Mallik, A. Masunov, T. Lazaridis, Distance and exposure dependent effective dielectric function, *J. Comput. Chem.* 23 (2002) 1090–1099.
- [21] Y. Okamoto, Dependence on the dielectric model and pH in a synthetic helical peptide studied by Monte Carlo simulated annealing, *Biopolymers* 34 (1994) 529–539.
- [22] V. Daggett, P. A. Kollman, I. D. Kuntz, Molecular dynamics simulations of small peptides: dependence on dielectric model and pH, *Biopolymers* 31 (1991) 285–304.
- [23] R. Constanciel, R. Contreras, Self consistent field theory of solvent effects representation by continuum models: Introduction of desolvation contribution, *Theoret. Chim. Acta. (Berl)* 65 (1984) 1–11.
- [24] W. C. Still, A. Tempczyk, R. C. Hawley, T. Hendrickson, Semianalytical treatment of solvation for molecular mechanics and dynamics, *J. Am. Chem. Soc.* 112 (1990) 61276129.

- [25] M. Califano, P. Harrison, Approximate methods for the solution of quantum wires and dots: Connection rules between pyramidal, cuboidal, and cubic dots, *J. Appl. Phys.* 86 (1999) 5054.
- [26] L. Serra, A. Puente, E. Lipparini, Orbital current mode in elliptical quantum dots, *Phys. Rev. B* 60 (1999) R13966–R13969.
- [27] K. Hirose, N. S. Wingreen, Spin-density-functional theory of circular and elliptical quantum dots, *Phys. Rev. B* 59 (1999) 4604.
- [28] G. Cantele, D. Ninno, G. Iadonisi, Confined states in ellipsoidal quantum dots, *J. Phys. Condens. Matter* 12 (2000) 9019–9036.
- [29] K. G. Dvoyana, E. M. Kazaryana, L. S. Petrosyan, Electronic states in quantum dots with ellipsoidal symmetry, *Physica E: Low-dimensional Systems and Nanostructures* 28 (2005) 333–338.
- [30] P. M. Morse, H. Feshbach, *Methods of Theoretical Physics*, McGraw-Hill, New York, 1953.
- [31] T. Miloh, Forces and moments on a tri-axial ellipsoid in potential flow, *Israel J. Tech.* 11 (1973) 63–74.
- [32] J. W. Perram, P. J. Stiles, On the application of ellipsoidal harmonics to potential problems in molecular electrostatics and magnetostatics, *Proc. R. Soc. Lond. A* 349 (1976) 125–139.
- [33] T. Miloh, Maneuvering hydrodynamics of ellipsoidal forms, *J. Ship Research* 23 (1979) 66–75.
- [34] J. C. E. Sten, Ellipsoidal harmonics and their application in electrostatics, *J. Electrostatics* 64 (2006) 647–654.
- [35] L. C. Lew Yan Voon, M. Willatzen, On triaxial ellipsoidal quantum dots, *J. Phys. Condens. Matter* 16 (2004) 1087–1093.
- [36] D. V. Redžić, An electrostatic problem: A point charge outside a prolate dielectric spheroid, *Am. J. Phys.* 62 (1994) 1118–1121.
- [37] S. Deng, Electrostatic potential of point charges inside dielectric prolate spheroids, *J. Electrostatics* 66 (2008) 549–560.
- [38] A. H. Sihvola, I. V. Lindell, Polarizability and effective permittivity of layered and continuously inhomogeneous dielectric spheres, *J. Electro. Waves Appl.* 3 (1989) 37–60.
- [39] A. H. Sihvola, I. V. Lindell, Polarizability and effective permittivity of layered and continuously inhomogeneous dielectric ellipsoids, *J. Electro. Waves Appl.* 4 (1990) 1–26.
- [40] I. V. Lindell, M. E. Ermutlu, A. H. Sihvola, Electrostatic image theory for layered dielectric sphere, *IEE Proc.-H* 139 (1992) 186–192.
- [41] A. H. Sihvola, I. V. Lindell, Transmission line analogy for calculating the effective permittivity of mixtures with spherical multilayer scatterers, *J. Electro. Waves Appl.* 2 (1988) 741–756.
- [42] J. C. de Munck, The potential distribution in a layered anisotropic spheroidal volume conductor, *J. Appl. Phys.* 64 (1988) 464–470.
- [43] C. Xue, S. Deng, Three-dielectric-layer hybrid solvation model with spheroidal cavities in biomolecular simulations, *Phys. Rev. E* 81 (2010) 016701.
- [44] E. W. Hobson, *The Theory of Spherical And Ellipsoidal Harmonics*, Cambridge University Press, Cambridge, England, 1931.
- [45] W. R. Smythe, *Static and Dynamic Electricity*, 3rd Edition, Hemisphere, New York, 1989.